QUANTITATIVE CONTROLS ON LOCATION AND ARCHITECTURE OF CARBONATE DEPOSITIONAL SEQUENCES: UPPER MIOCENE, CABO DE GATA REGION, SE SPAIN

EVAN K. FRANSEEN[1], ROBERT H. GOLDSTEIN[2], AND MARK R. FARR[2]
[1] *Kansas Geological Survey, University of Kansas, 1930 Constant Ave., Lawrence, Kansas 66047, U.S.A.*
[2] *University of Kansas, Department of Geology, 120 Lindley Hall, Lawrence, Kansas 66045, U.S.A.*

ABSTRACT: **Sequence stratigraphy, pinning-point relative sea-level curves, and magnetostratigraphy provide the quantitative data necessary to understand how rates of sea-level change and different substrate paleoslopes are dominant controls on accumulation rate, carbonate depositional sequence location, and internal architecture. Five third-order (1–10 my) and fourth-order (0.1–1.0 my) upper Miocene carbonate depositional sequences (DS1A, DS1B, DS2, DS3, TCC) formed with superimposed higher-frequency sea-level cycles in an archipelago setting in SE Spain.**

Overall, our study indicates when areas of high substrate slope ($>$ 15°) are in shallow water, independent of climate, the location and internal architecture of carbonate deposits are not directly linked to sea-level position but, instead, are controlled by location of gently sloping substrates and processes of bypass. In contrast, if carbonate sediments are generated where substrates of low slope ($<$ 15° in our area) are in shallow water, then architecture and location of deposits may be more directly controlled by the relative position of sea level. For these systems, the rates of relative sea-level change are important for determining which systems tracts develop.

DS1A–DS1B, cooler-water ramps, result from sediment bypass across steep paleoslopes to toes of slopes. Accumulation rates decreased from $>$ 15.6 cm/ky to $\sim$ 2 cm/ky and overall relative sea level rose at rates of 17–21.4 cm/ky. Higher frequency sea-level rates were about 111 to more than 260 cm/ky, producing onlapping, fining- (deepening-) upward cycles. Decreasing accumulation rates resulted from decreasing surface area for shallow-water sediment production, drowning of shallow-water substrates, and complex sediment dispersal related to the archipelago setting. Typical systems tract and parasequence development should not be expected in ''bypass ramp'' settings; facies of onlapping strata do not track base level and are likely to be significantly different compared to onlapping strata associated with coastal onlap.

Basal and upper DS2 reef megabreccias (indicating the transition from cool to warmer climatic conditions) were eroded from steep upslope positions and redeposited downslope onto areas of gentle substrate during rapid sea-level falls ($>$ 22.7 cm/ky) of short duration. Such rapid sea-level falls and presence of steep slopes are not conducive to formation of forced regressive systems tracts composed of downstepping reef clinoforms.

The DS3 reefal platform formed where shallow water coincided with gently sloping substrates created by earlier deposition. Slow progradation (0.39–1.45 km/my) is best explained by the lack of an extensive bank top, progressively falling sea level, and low productivity resulting from siliciclastic debris and excess nutrients shed from nearby volcanic islands. Although DS3 strata were deposited during a third-order relative sea-level cycle, a typical transgressive systems tract is not recognizable, indicating that the initial relative rise in sea level was too rapid ($\gg$ 19 cm/ky). Downstepping reefs, forming a forced regressive systems tract, were deposited during the relative sea-level fall at the end of DS3, indicating that relatively slow rates of fall (10 cm/ky or less) over favorable paleoslope conditions are conducive to generation of forced regressive systems tracts consisting of downstepping reef clinoforms.

The TCC sequence consists of four shallow-water sedimentary cycles that were deposited during a 400 ky to 100 ky time span. Such shallow-water cycles, typical of many platforms, form only where shallow water intersects gently sloping substrates. The relative thicknesses of cycles ($<$ 2 m to 15 m thick), magnitudes of relative sea-level fluctuations associated with each cycle (25–30 m), high rates of relative sea-level fluctuations (minimum of 25–120 cm/ky), and the widespread distribution of similar TCC cycles in the Mediterranean and elsewhere are supportive of a glacio-eustatic influence. With rates of sea-level change so high, typical systems tracts do not form.

INTRODUCTION

Recent sequence-stratigraphic studies of shallow-water carbonates have focused increasingly on higher-resolution ($<$ 1–10 my; $>$ third order) sequence-stratigraphic frameworks and determining the variables that control sequence and cycle development (e.g., Pomar 1991; Franseen et al. 1993; Sonnenfeld and Cross 1993; Goldhammer et al. 1993; Reid and Dorobek 1993; Gianniny and Simo 1996; Grammar et al. 1996; Franseen and Goldstein 1996). Many studies have shown that relative sea-level variations are important in controlling sequence architecture (see Sarg 1988; Handford and Loucks 1993; Burchette and Wright 1992 for reviews and examples). However, other variables need investigation, such as climate, sediment accumulation rates, rates of sea-level change, paleoslope, and paleo-oceanographic conditions, to show how they affect carbonate sequences. Even though some of these variables have been studied, they have yet to be thoroughly evaluated quantitatively. Quantification of the variables is achieved with a detailed description of depositional sequences, reconstruction of paleotopography, developing the chronostratigraphy, and reconstruction of the quantitative relative sea-level history. With these data, comparisons with other basins can differentiate local, regional, and global controls.

Although biostratigraphy is commonly used for chronostratigraphic information in studies of carbonate platforms, typically it does not provide the resolution that is necessary for evaluating high-resolution sequence-stratigraphic frameworks and quantifying variables such as accumulation rate and progradation rate. Magnetostratigraphy holds potential as a useful alternative or complement to biostratigraphy. Some paleomagnetic studies of shallow-water carbonates can be made difficult by extremely low natural remanent magnetizations (NRM $< 10^{-9}$ A·m^2/kg; e.g., Lowrie and Heller 1982), magnetic overprinting by recent viscous remanent magnetization (VRMs), recent hematization, or discontinuous sedimentation (Quinn and Matthews 1990). Despite these difficulties, recent studies have been successful in establishing magnetic reversal stratigraphies within carbonates (e.g., McNeill et al. 1988; Aissaoui et al. 1990; Cunningham et al. 1994). For most of the successful studies the magnetic carriers are single-domain to pseudo-single-domain magnetite grains which are, in part, the product of magnetotactic bacteria (Aissaoui et al. 1993). Our study employs magnetostratigraphy of upper Miocene carbonate rocks that formed during a period of rapid magnetic reversals (approximately 1 reversal per 180,000 years). In addition, the samples possess high NRM (typically $> 10^{-7}$ A·m^2/kg) because of admixed volcaniclastic debris from nearby volcanic basement highs, greatly reducing many of the problems in magnetostratigraphic work on carbonates.

This study is the first to establish a reliable high-resolution chronostra-

JOURNAL OF SEDIMENTARY RESEARCH, VOL. 68, NO. 2, MARCH, 1998, P. 283–298
 1073-130X/98/068-283/$03.00

tigraphy utilizing magnetostratigraphy and radiometric dating, a high-resolution sequence-stratigraphic framework, and detailed quantitative relative sea-level curves for Tortonian cool-water to Tortonian–Messinian warm-water carbonate platforms of the Mediterranean region. Results provide high-resolution information on magnitudes and timing of relative sea-level fluctuations, rates of relative sea-level change, accumulation rates, and progradation rates. When these are compared to the record of climate, detailed sequence architecture, and substrate paleoslope, they are useful in developing quantitative constraints on the variables that controlled depositional sequence architecture and location. This well-constrained example can be compared to other regions to evaluate the local, regional, and global controls on sequence development.

Our results indicate that rate of relative sea-level change and paleoslope are important controls on sequence architecture, which cause deviations away from traditional systems tracts models. In this system, accumulation rates are not just a function of water depth but are controlled, at least in part, by (1) the area of shallow-water substrate, (2) complex sediment dispersal patterns affected by substrate paleoslope, and (3) proportion of ''drowned'' substrate. Moreover, reef progradation rate and geometry are affected by position of sea level, rate of relative sea-level change, substrate paleotopography, siliciclastic input, and area available for shallow-water carbonate production.

In addition to understanding global, regional, and local controls on the upper Miocene stratigraphic record of the Mediterranean, our results on the controlling factors for carbonate sequence development in this area of variable substrate paleoslope should have application for carbonate sequence-stratigraphic studies in similar settings, such as margins of carbonate platforms, archipelagos, and other oceanic islands. Finally, this study may have specific applications to carbonate ramp and platform studies in general because: (1) it evaluates controls on platform evolution from a temperate ramp to tropical reef; temperate water carbonates are increasingly being recognized in the geologic record (James and Clarke 1997); and (2) on most carbonate platforms, there are likely to be times when areas of high substrate slope are in shallow water.

GEOLOGIC SETTING

The study area is located in the Cabo de Gata region of Spain, on the southern margin of the Almeria Basin (Fig. 1). A strike-slip fault (Carboneras Fault), active throughout Tortonian, Messinian, and Pliocene times (Montenat et al. 1987), separates Neogene volcanic basement in the Cabo de Gata region to the southeast from Mesozoic–Paleozoic basement of the Betic Range to the northwest. Most of the volcanic rocks are older than the upper Miocene carbonate sequences, although locally interbedded volcanic units have been identified in the lowest carbonate depositional sequence (Franseen and Goldstein 1992; Franseen et al. 1993; Franseen and Goldstein 1996; Franseen et al. 1997). The interbedded volcanic unit in this lowest sequence (DS1A; Fig. 2) yielded an $^{40}Ar/^{39}Ar$ date of 8.5 $\pm$ 0.1 Ma (Goldstein and Franseen 1995; Franseen and Goldstein 1996), which provides an important absolute date for the magnetostratigraphy. The older Neogene volcanic basement rocks formed an archipelago (Esteban 1979, 1996) and the carbonate sequences were deposited on the flanks of those volcanic hills, which had variable slope angles. All of the carbonate sequences analyzed in this study contain detrital volcanic fragments that were shed from the volcanic highs (Franseen 1989; Franseen et al. 1993).

Prior work has established a well-defined sequence-stratigraphic framework and quantified relative sea-level history for the carbonate units in the Cabo de Gata area (Franseen 1989; Franseen and Mankiewicz 1991; Franseen and Goldstein 1992; Franseen et al. 1993; Goldstein and Franseen 1995, Franseen and Goldstein 1996; Franseen et al. 1997). The following is primarily a summary of these studies.

Five depositional sequences have been identified within the upper Miocene carbonate complex in the area. We define the sequences based on direct and indirect lines of evidence of relative sea-level falls at each sequence boundary (SB in Figure 2). The lower two sequences (DS1A and DS1B) are carbonate ramps that generally onlap against irregular volcanic basement topography. A well-defined subaerial exposure surface separates underlying volcanic basement from DS1A, the lowest sequence. DS1A varies from 0 to 20 m in thickness and consists mainly of bryozoan-rich facies, minor red-algal packstone, and, locally, volcaniclastic-rich sandstone and conglomerate (Fig. 2). DS1A strata were deposited during an overall rise of at least 25–30 m in inner and outer ramp settings in cool water resulting from a temperate climate and possibly coinciding with upwelling.

Lower DS1B strata were deposited on a surface of subaerial exposure (sequence boundary) at the top of DS1A, and volcanic basement. DS1B varies from 20 to more than 100 m in thickness and generally onlaps DS1A and volcanic basement up to a present-day elevation of about 150 m. DS1B consists of at least six upward-fining (upward-deepening) cycles (2–15 m in thickness) composed of basal cross-bedded, graded, or slump-brecciated red-algae-rich packstone/grainstone that fines upward to foraminiferal wackestone/packstone; detrital volcanic fragments are present throughout the cycles. Upper DS1B strata contain the earliest significant amounts of chlorozoan grains in the platform. DS1B strata indicate deposition during an overall rise in sea level of at least 150 m with at least six superimposed higher-frequency fluctuations. DS1B ramp strata exhibit onlap caused by carbonate production, reworking, and accumulation at toes of slopes in water depths of 40 to 100+ m, and from carbonate sediments produced updip that were bypassed across steep basement slopes to accumulate at the toes of slopes. The facies suggest deposition during a shift from cooler to warmer water associated with temperate to subtropical climate conditions, possibly in conjunction with upwelling.

The sequence boundary at the base of DS2 is placed at the base of a unit consisting of megabreccia clasts (MB1) composed primarily of reef facies with *Tarbellastraea* and *Porites* corals (Fig. 2). Clasts show evidence of transport including tilted and rotated geopetal orientations, scoured bases, and soft-sediment deformation of underlying and adjacent strata. The MB1 clasts likely originated as upslope reefs. Although no subaerial exposure evidence has been identified at the base of MB1, some clasts of MB1 contain evidence of subaerial exposure prior to transport, thereby indicating a relative sea-level fall associated with erosion and transport. The sediments flanking the megabreccia blocks are typically skeletal grainstones. Overlying these are some packstones/grainstones but mostly foraminiferal wackestone. The thickness of DS2 varies from 1 to 30 m. DS2 strata mostly drape gently sloping ramp surfaces created by earlier deposition and have facies reflecting the continuation of subtropical or tropical conditions.

The basal DS3 sequence boundary is a sharp erosional surface that locally is associated with a second megabreccia unit (MB2; Fig 2) composed primarily of *Porites* boundstone clasts and debris. MB2 clasts originally grew as DS2 reefs in upslope locations. However, an initial relative drop in sea level resulted in erosion and downslope redeposition of the reef material (Franseen et al. 1993). Subaerial exposure features on top of MB2 indicate that sea level continued to drop to expose the redeposited material in distal slope positions. Because the base of MB2 correlates with the initial relative fall in sea level and the upper MB2 surface represents later stages of the same relative sea-level drop, the upper DS2/basal DS3 sequence boundary is best defined as a *zone* encompassing the entire MB2 unit and the surfaces above and below it (Fig. 2). DS3 ranges in thickness from 20 to 70 m. It consists primarily of low- to high-angle, progradational and aggradational, reef-complex strata; later stages are characterized by downstepping progradational geometries formed in response to a falling relative sea level, with in-place reefs that formed on the forereef slopes of previous reef cycles (Fig. 3). The reef complex is characterized by minor in-place *Porites* reef core facies but is composed predominantly of downlapping forereef slope strata. These strata comprise coarse-grained and fine-grained skeletal packstones/grainstones mostly consisting of *Porites*, red algae, and

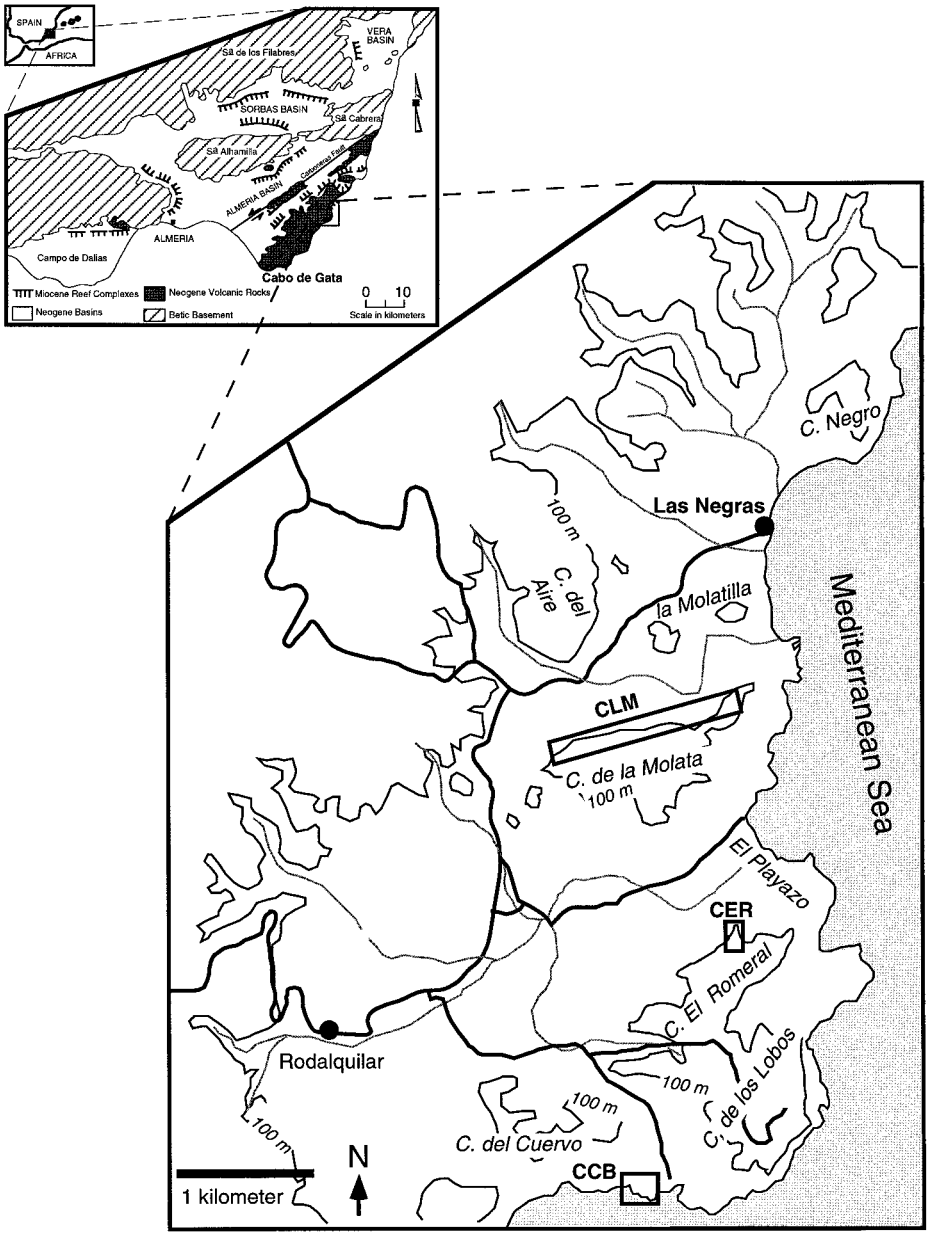

FIG. 1.—Location map of study area, showing regional geology and sample site locations. CCB, CER, CLM refer to sample site designations for Cerro del Cuervo Beach, Cerro El Romeral, and Cerro de La Molata, respectively.

mollusc fragments, and reef boundstone clasts. Finer-grained packstones/grainstones typically are present in more distal positions. There are eight or so separate reef cycles preserved, and several of these cycles developed on thick wedges of volcaniclastic debris (fan delta lobes). The position of the earliest in-place DS3 reefs indicate a relative rise in sea level of at least 150 m. Later downstepping DS3 reef progradation and a subaerial exposure surface developed on top of DS3 strata indicate a relative sea-level fall of at least 110 m. DS3 reefs are preserved only above relatively gentle substrate slopes, mostly created by earlier deposition. The DS3 coral reef strata indicate deposition in a subtropical to tropical climate.

The upper sequence, Terminal Carbonate Complex (TCC), overlies the subaerial exposure surface (sequence boundary) present on top of DS3. TCC ranges up to 30 m in thickness and consists of four normal- to restricted-marine shallow-water cycles ranging from < 2 to $15+$ m thick. The cycles are characterized by stromatolitic carbonates at the base that pass upward to fossiliferous packstone and cross-bedded oolite that may become fenestral towards the top. Each cycle is capped by a subaerial-exposure surface. TCC strata drape minor preexisting topography but are best preserved overlying relatively gently sloping substrates created by earlier deposition and erosion. The TCC was deposited after, and perhaps partially in conjunction with, basinal evaporite deposition (Esteban 1979; Rouchy 1982; Rouchy and Saint-Martin 1992; Esteban 1996). Initial TCC deposition indicates a minimum relative sea-level rise of 100 m and relative sea-level fluctuations on the order of 30 m during deposition of each cycle within the TCC. The TCC depositional sequence is capped by a subaerial-exposure surface (sequence boundary) indicating a relative sea-level fall of at least 200 m. TCC lithofacies reflect normal to restricted marine, subtropical/tropical conditions.

PALEOMAGNETIC METHODS

Sampling Strategy

Oriented hand samples or cores were collected for paleomagnetic study from 336 stratigraphic horizons at the Cerro del Cuervo Beach, Cerro El

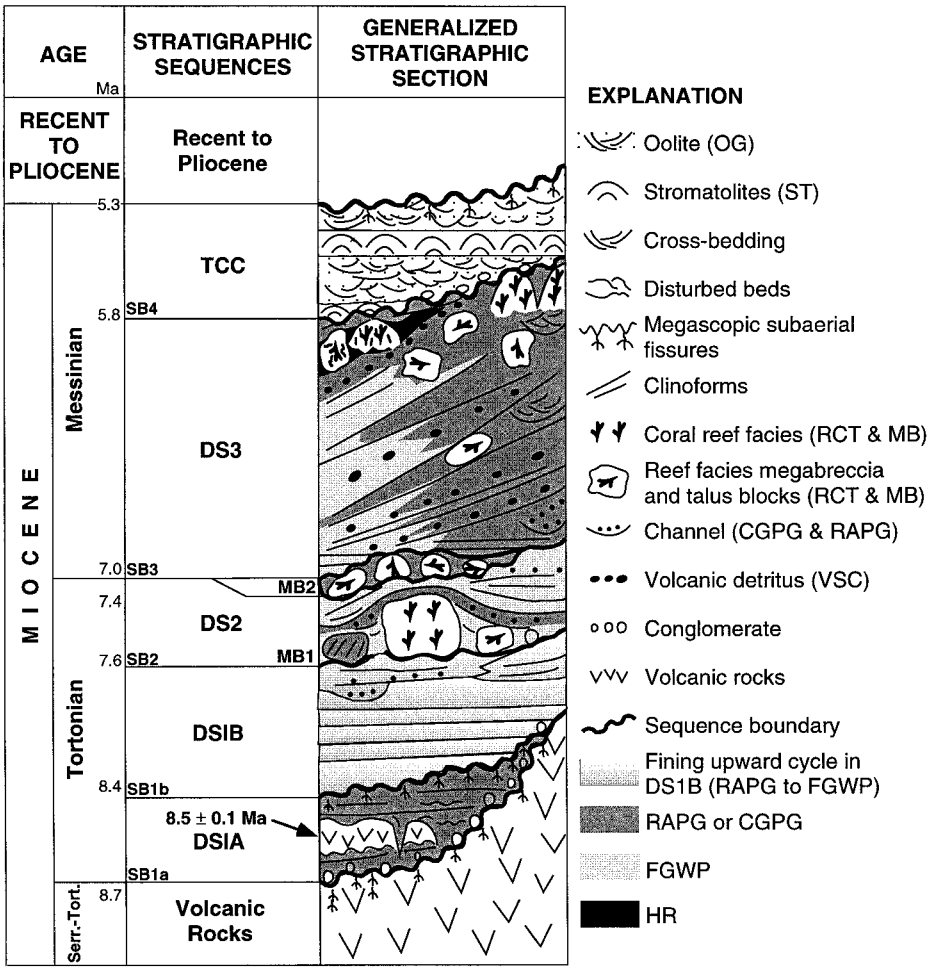

FIG. 2.—Generalized stratigraphic section of the depositional sequences in the Cabo de Gata area, showing ages as determined from paleomagnetic data and a radiometrically dated volcanic unit in DS1A. Symbols and patterns illustrate generalized facies relationships. OG = oolitic grainstone, ST = stromatolite boundstone, RCT = reef core/talus, MB = megabreccia, CGPG = coarse-grained packstone/grainstone, RAPG = red-algae packstone/grainstone, VSC = volcanic sandstone/conglomerate, FGWP = fine-grained wackestone/packstone, HR = *Halimeda* rich. SB = sequence boundary, which we define on the basis of evidence for relative sea-level falls.

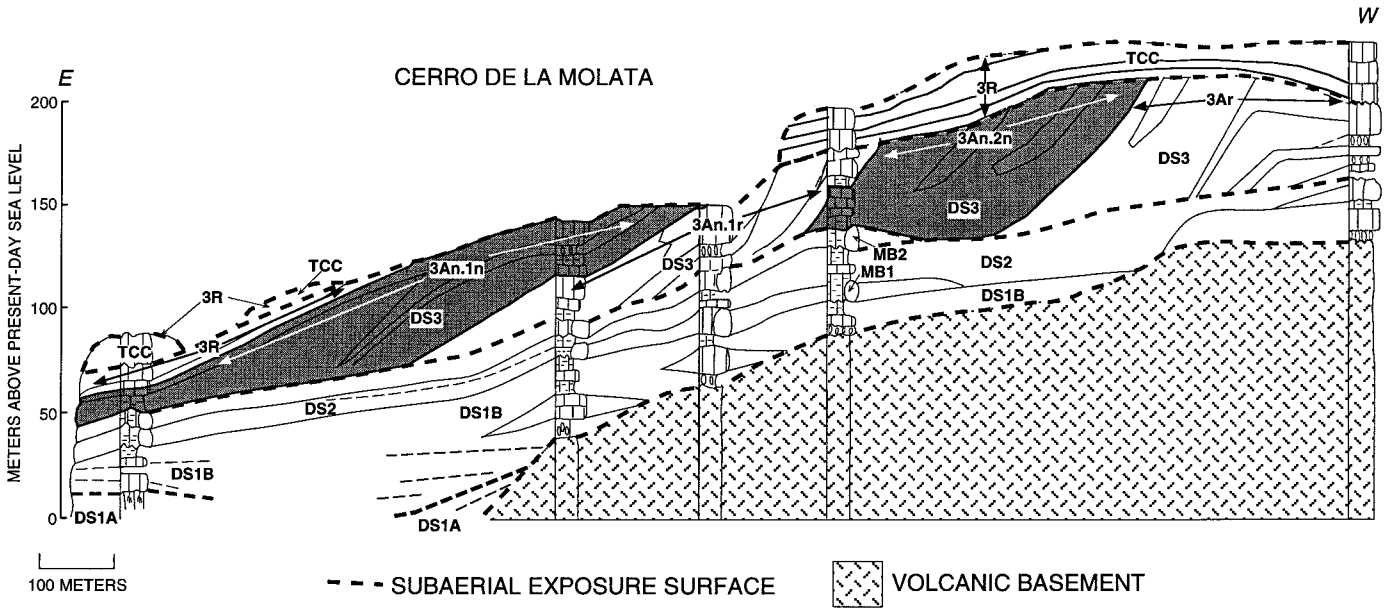

FIG. 3.—Cross section of the La Molata outcrop (location CLM on Figure 1), showing magnetostratigraphy for DS3 and TCC strata. See Figures 4 and 6 for magnetostratigraphy of the earlier sequences.

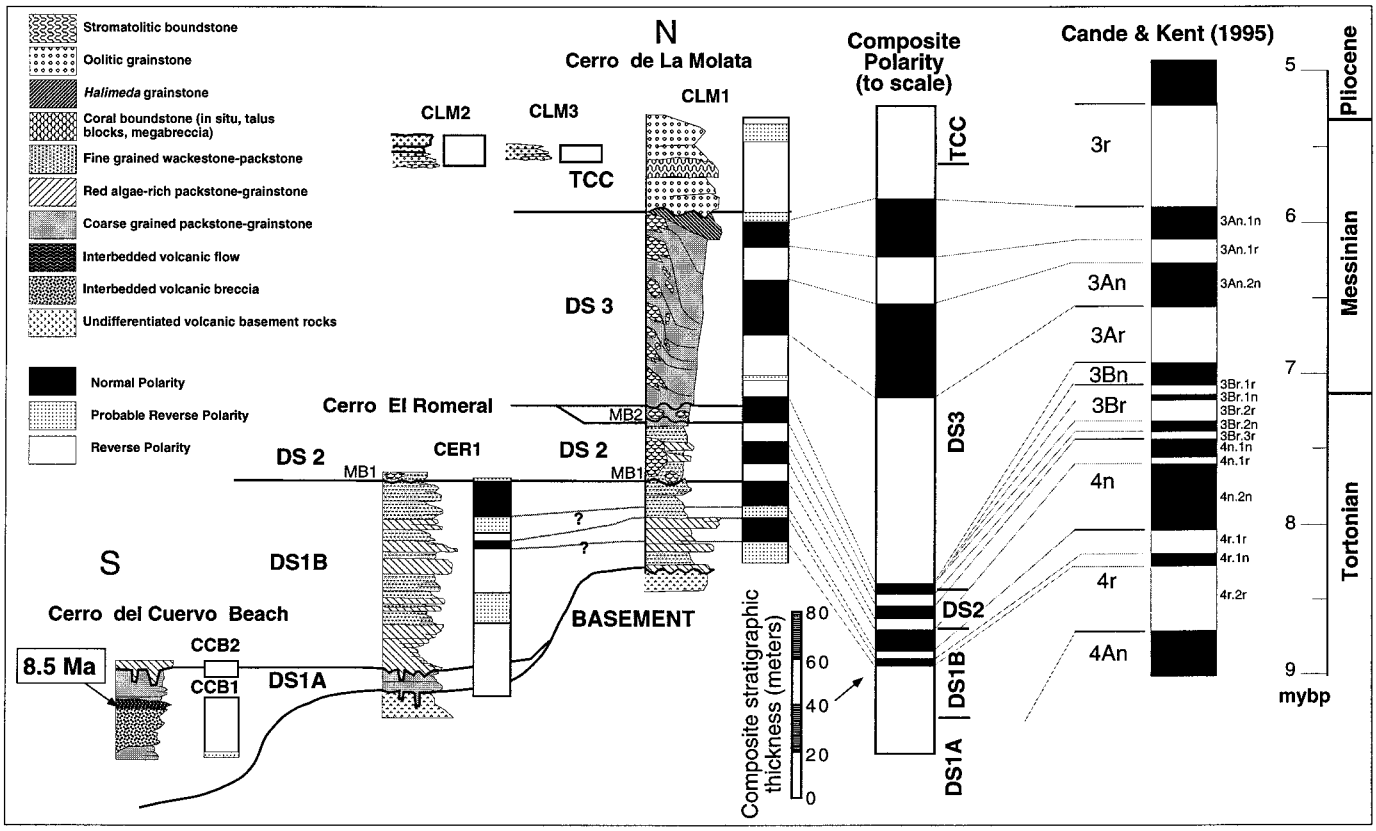

FIG. 4.—Stratigraphic correlation of reversal stratigraphy of all sample sites used to construct the resultant interpreted composite polarity and our interpretation of its correlation to the GPTS of Cande and Kent (1995).

Romeral, and Cerro La Molata outcrop localities (CCB, CER, CLM, respectively, in Figure 1). Samples from fissure-fill sediments at the sequence boundary between DS1A and the Neogene volcanic basement rocks at Cerro El Romeral and at the upper DS1A sequence boundary at Cerro del Cuervo Beach were collected in order to obtain a more complete stratigraphic record across those sequence boundaries, and also to approximate the duration of the hiatus at the sequence boundaries. Sequence DS1A was sampled at both the Cerro del Cuervo Beach and Cerro El Romeral localities. Samples from sequence DS1B were collected from all three localities. Seventy-three stratigraphic horizons were sampled along an 1800 m west-to-east transect along the tops of clinoforms of sequence DS3 at Cerro de La Molata (Fig. 3). These sample localities were positioned in order to obtain the most complete stratigraphic coverage, from oldest to youngest clinoforms. TCC samples were obtained from the top of Cerro de La Molata as well as from two isolated in-place remnants of TCC present at lower elevations east of and down depositional dip from the main TCC outcrop (Fig. 3).

Sample Analysis

Stepwise demagnetization and measurement of remanences were performed on approximately 405 specimens. Both thermal demagnetization (to 700°C) and alternating field (AF) demagnetization (to 90 mT) were used either separately or in combination. Remanences were measured using a two-axis cryogenic magnetometer housed in a magnetically shielded room. Isothermal remanent magnetization (IRM) acquisition and thermal demagnetization was used to characterize likely magnetic mineral carriers. Principal component analysis (Kirschvink 1980) was used to determine characteristic paleomagnetic directions for all samples.

IRM acquisition and thermal demagnetization suggest that most lithologies are dominated by one or more low-coercivity magnetic phases that have maximum unblocking temperatures of around 575°C. Thus, low-titanium magnetite, which has a Curie temperature of 580°C, is likely the dominant magnetic phase. Importantly, most samples with either stable normal or reversed directions possess this same IRM acquisition and demagnetization behavior.

Further details, including data and sample locations for the paleomagnetic portion of the study, are presented in a separate study (Farr et al., unpublished data) and are available upon request.

MAGNETOSTRATIGRAPHY

The record of magnetic reversal stratigraphy in the study area can be correlated locally and regionally, and can be related to an absolute time scale through correlation to the global paleomagnetic record. Reversal stratigraphies for stratigraphic sections from various hills in the area show consistent records for each depositional sequence. Figure 4 illustrates the correlation of each chron. Average thicknesses of the various intervals can be used to construct a composite stratigraphic section of magnetic reversals. This composite polarity (Fig. 4) is used to correlate the local record to other regions and to the global record of magnetic reversals.

The reversal stratigraphy in the Cabo de Gata area is tentatively correlated to the global polarity time scale (GPTS) of Cande and Kent (1995) and to reversal stratigraphies of similar-aged units in the Melilla basin in Morocco and to the Sorbas basin northeast of the field area (Fig. 4; Farr et al., unpublished data). On the basis of the radiometric date of 8.5 $\pm$ 0.1 Ma for the interbedded volcanic flow in DS1A, a chron 4r.2r age can be assigned to the long reversed interval in sequences DS1A and DS1B. A 3r chron age is assigned to the reversed TCC section of this study on the basis of its relationship with immediately overlying Pliocene strata (the start of

the Pliocene has been given an age of 5.32 Ma, Cande and Kent 1995) and on regional data on the TCC (e.g., Sorbas basin; Gautier et al. 1994). Therefore, the rest of the reversal stratigraphy in DS1B, DS2, and DS3 must correspond to chrons 4n to 3Ar (Fig. 4). Biostratigraphic dating of strata in the Cabo de Gata area is poor because of the scarcity and poor preservation of age-diagnostic fossils. The limited biostratigraphy available (Serrano 1992; Franseen and Mankiewicz 1993) is consistent with our radiometric and magnetostratigraphic data.

There are thirteen chrons within the study interval in the Cabo de Gata area, as compared with a total of seventeen in the GPTS (Fig. 4). An important question is which unconformities account for the missing chrons. In the absence of any evidence of a significant unconformity or surface of nondeposition within DS1B, the two normal intervals within upper DS1B suggest a correlation with chron 4n from Cande and Kent (1995; Fig. 4). Correlations of reversals within sequence DS2 and the lower part of DS3 are more problematical because of a lack of age control. The most reasonable interpretation (Fig. 4) assumes that the record of chrons 3Br.2r through 3Bn is missing and corresponds to *in situ* subaerial exposure of MB2 and sediment starvation associated with the downlap surface at the base of DS3. Sequence DS2 would correspond to the upper two chrons of 4n and the lowest reversed chron within 3Br, and the normal MB2 interval would correlate with chron 3Br.2n (Fig. 4). This magnetostratigraphy suggests that the subaerial exposure and sediment starvation on top of MB2 represents at least 406,000 years.

The proposed correlation to the GPTS is supported by biostratigraphic, sequence stratigraphic, and magnetostratigraphic correlations to other regions of the Mediterranean. In our interpretation, the upper three chrons in DS3 correspond to chron 3An in the GPTS. A similar reef-complex depositional sequence in the Melilla basin of northern Morocco has been assigned a chron 3An age by Cunningham et al. (1994). The Melilla basin correlations to the GPTS are further constrained by the first appearance of the index fossil *Globorotalia conomiozea* within chron 3Ar and by six radiometric dates of volcanics within the section (Cunningham et al. 1994). The TCC in our study area is interpreted to fall within chron 3r (Figs. 3, 4). Throughout the western Mediterranean, TCC deposition is typically interpreted to have occurred after, and perhaps partially during, basinal evaporite deposition of the Messinian salinity crisis (Esteban 1979, 1996; Rouchy 1982; Rouchy and Saint Martin 1992; Clauzon et al. 1996), which occurred entirely within chron 3r (e.g., Channell et al. 1990). With this correlation as a basis, the published data suggest between 400 ky and 100 ky for TCC deposition.

Accumulation Rates

Plots of age versus stratigraphic thickness for the depositional sequences illustrate the varying rates of accumulation using the correlation scheme to the GPTS (Fig. 5). Although at least minor compaction is likely to have occurred, we made no correction for compaction because of the lack of stylolites, pressure-solution features, or other evidence of significant compaction. In addition, the section was probably never deeply buried (Addicott et al. 1978; Franseen 1989). Accumulation rates determined from the magnetic reversal stratigraphy of DS1A and DS1B have been reported previously by Franseen et al. (1997). In order to translate progradational accumulation in DS3 to a proxy for vertical accumulation, thickness normal to clinoform bedding was calculated trigonometrically along the sequence boundary capping DS3. It is important to note that the values for DS3 are best regarded as rough estimates because of thickness changes along clinoforms and because of error in the trigonometric conversion caused by variable dips along clinoforms.

The accumulation rate for upper DS1A and lower DS1B (top of 8.5 Ma volcanic flow to chron 4r.1n) is $>$ 15.6 cm/ky (Fig. 5). This rate is a minimum because of the unconformity at the top of DS1A. The next higher two chrons of DS1B indicate accumulation rates of 10.9 cm/ky (chron 4r.1n) and 1.9 cm/ky (chron 4r.1r). It is important to note that, although the paleomagnetic data in 4r.1n and 4r.1r have the greatest ambiguities for determining polarity, possible scenarios for shifting their positions would produce similar low accumulation rates. The accumulation rate calculated for 4n.2n is $\geq$ 2.2 cm/ky. Although the accumulation rate for that interval should be regarded as a minimum because there is a sequence boundary at its top, there is little evidence for erosion or nondeposition, so the value may be close to the actual accumulation rate. Therefore, the DS1A and DS1B succession is interpreted to record generally decreasing accumulation rates through time from at least 15.6 cm/ky to about 2 cm/ky (Fig. 5).

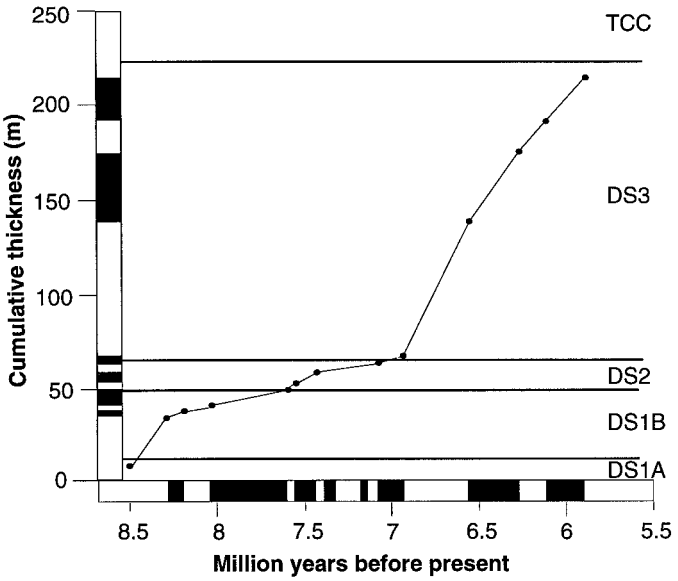

FIG. 5.—Plot of age versus cumulative thickness of the composite reversal stratigraphy from this study indicating accumulation rates. Steep slopes indicate more rapid accumulation.

For the correlation between the GPTS and DS2 (Fig. 4), the base of chron 4n.1r corresponds to the base of DS2 and gives an accumulation rate of $\geq$ 7.4 cm/ky. Even though stratigraphic and paleomagnetic evidence argues against significant erosion or nondeposition at the basal DS2 sequence boundary, this rate should be considered a minimum because there is likely to be some missing record. The only normal chron within DS2 corresponds to chron 4n.1n and indicates an accumulation rate of 3.5 cm/ky. The top of DS2 corresponds to chron 3Br.3r and indicates an accumulation rate of $\geq$ 8.8 cm/ky. The top of this chron abuts the base of MB2 (the base of a sequence boundary zone); there is little evidence for significant erosion or nondeposition here, but the rate should still be regarded as a minimum.

The accumulation rate for MB2 is a minimum because it contains only one chron and is bounded below by a surface correlative to a relative fall in sea level (base of the sequence boundary zone) and above by a surface of subaerial exposure and downlap (top of the sequence boundary zone). The rate calculated for MB2 is $>$ 11.2 cm/ky (Fig. 5).

DS3 reef complex strata contain 4 chrons and a part of another. Lower DS3 strata correlate to chron 3Ar and have an accumulation rate of $>$ 21.8 cm/ky (Fig. 5). Because the lower DS3 sequence boundary coincides in part with this chron, this rate should be regarded as a minimum. Overlying DS3 strata correspond to chron 3An.2n and yield an accumulation rate of 13.4 cm/ky (Fig. 5). The 3rd chron in DS3 corresponds to chron 3An.1r, which gives an accumulation rate of 15.1 cm/ky (Fig. 5). The youngest full DS3 chron corresponds to chron 3An.1n, which yields an accumulation rate of 10.3 cm/ky (Fig. 5). The uppermost part of DS3 corresponds to chron 3r, but because this chron crosses the major sequence boundary at

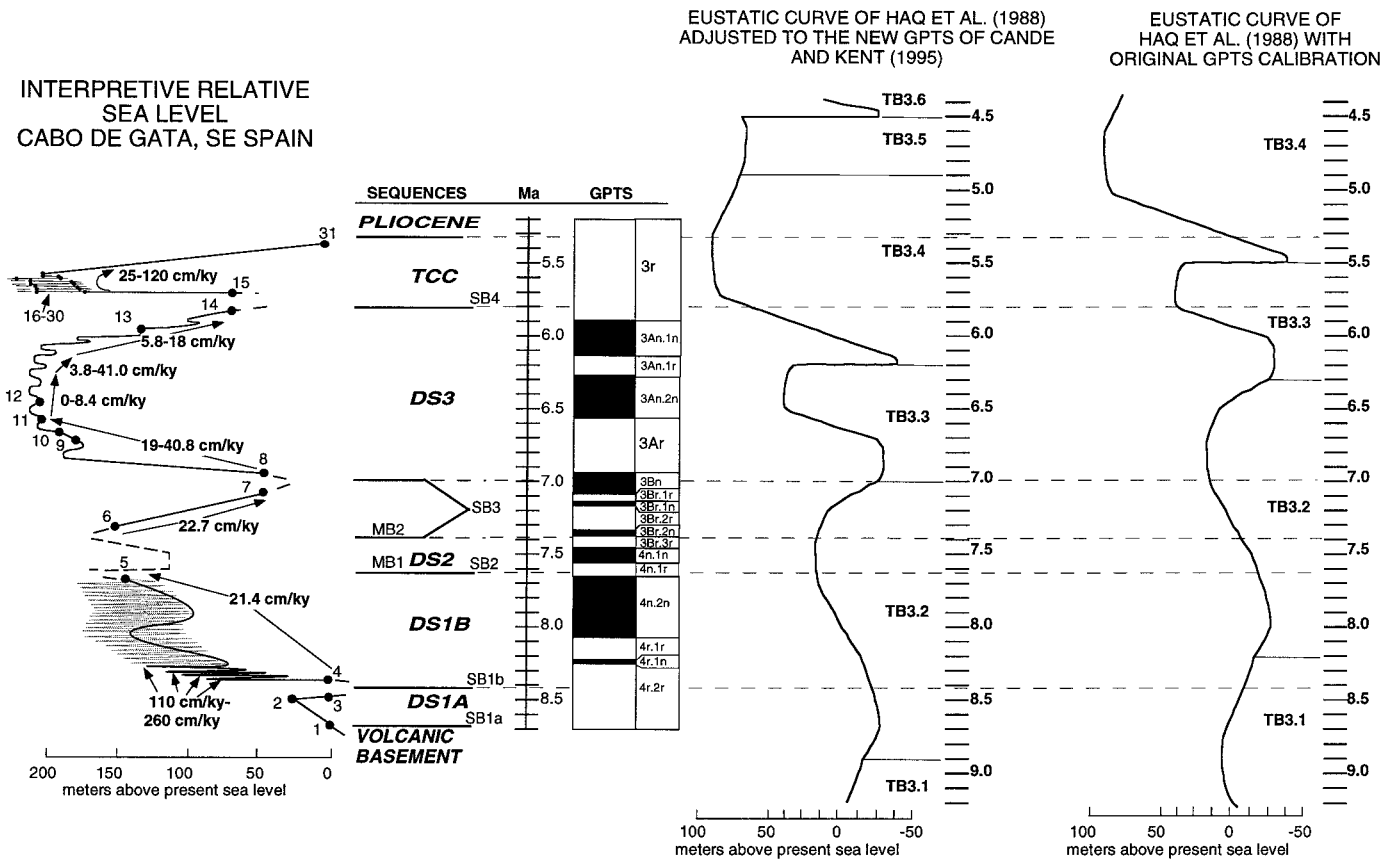

FIG. 6.—Interpretive relative sea-level curve with pinning points and rates of sea-level fluctuations from Cabo de Gata, SE Spain calibrated to the GPTS of Cande and Kent (1995). Numbers on the interpretive curve are pinning points, which are known positions of relative sea level (see Goldstein and Franseen 1993, Franseen et al. 1993, and Goldstein and Franseen 1995 for further details on pinning points and construction of the Cabo de Gata relative sea-level curve). Note that the DS1B part of the curve reflects two different interpretations of sea-level history discussed in the text. The interpretive curve is compared to the eustatic curve of Haq et al. (1988) recalibrated to the GPTS of Cande and Kent (1995) and to the original curve of Haq et al. (1988).

the top of DS3 and continues into TCC deposition, an accumulation rate cannot be calculated for these strata.

Determining accumulation rates for TCC strata is difficult because: (1) TCC strata are bounded below and above by sequence boundaries; (2) TCC falls entirely within chron 3r, which continues into underlying beds; and (3) each of the four TCC cycles are bounded by subaerial exposure surfaces. Nevertheless, a bare minimum rate of 5.2 cm/ky can be calculated for TCC using the time interval between the 5.32 Ma age of the beginning of the Pliocene (Hilgen and Langereis 1993; Cande and Kent 1995) and the age of the beginning of chron 3r. TCC strata are likely to have been deposited during a much shorter time than this. They typically are thought to correlate, at least partially, with the Upper Evaporite unit of the basin (e.g., Esteban 1979, 1996; Rouchy 1982; Rouchy and Saint Martin 1992; Clauzon et al. 1996), which would suggest between 400 ky and 100 ky for TCC deposition. These age considerations yield accumulation rates ranging from 7.5 cm/ky to 30.0 cm/ky for TCC in our area. These estimates are still minima because of the cycle-bounding surfaces of subaerial exposure within TCC.

Progradation Rates

Progradation rates for the reef complex facies of DS3 are calculated using the horizontal distance of progradation normal to the strike of prograding beds. Progradation is measured at the sequence boundary capping DS3. Using chrons 3Ar to the end of 3An.1n (Fig. 3), the entire DS3 platform prograded 935 m during 1.04 my to yield an overall progradation rate of 0.90 km/my. DS3 strata of chron 3Ar initially aggraded and finally prograded yielding a minimum progradation rate of 0.39 km/my. Strata of 3An.2n yield a progradation rate of 1.02 km/my; 3An.1r strata yield a rate of 1.45 km/my; and the strata of 3An.1n yield a rate of 1.21 km/my.

Rates of Relative Sea-Level Change

Time calibration of the pinning-point interpretive relative sea-level curve allows rates of relative sea-level change to be determined (Fig. 6). This curve contains both well-controlled quantitative constraints on relative sea level (pinning points) and other information on relative sea level based on interpretations from the lithofacies (Franseen et al. 1993; Goldstein and Franseen 1995). A precise rate of rise for DS1A is difficult to calculate because it contains no chron boundaries. An overall rate of relative sea-level rise can be calculated from the 8.5 Ma volcanic unit in DS1A to the pinning point at the top of DS1B, which approaches the top of chron 4n.2n. This yields a rate of rise of 17.6 cm/ky, which should be regarded as a minimum because of the two sequence boundaries in this interval. An overall minimum rate of rise of 21.4 cm/ky is calculated just for DS1B strata from a pinning point near the base of chron 4r.1n to a pinning point near the top of 4n.2n. DS1B contains six fining-upward cycles, which have been interpreted from lithofacies to represent deepening-upward cycles. Bases of cycles are interpreted to have been deposited in 40–100 m of water and tops of cycles in depths greater than 100 m (Franseen and Goldstein 1996; Franseen et al. 1997). The lower approximately four and one half cycles were deposited during chron 4r.2r. Using the 8.5 Ma date on the interbed-

ded volcanic unit in DS1A and the age of the end of chron 4r.2r, we derive a maximum average cycle duration of 54 ky. Because this time interval includes DS1A deposits and a sequence boundary, the average cycle duration is probably considerably less. Using linear relative sea-level rises and falls of 70, 50, and 30 m, respectively, for each cycle (each is plausible based on depth of deposition ranges for the facies), the minimum rates of sea-level change were 260 cm/ky, 185 cm/ky, and 111 cm/ky, respectively. Although the preservation of the paleomagnetic signal is poorest in the fifth and sixth cycles of DS1B, the upper part of cycle five appears to have been deposited during all of chron 4r.2r, 4r.1r and perhaps the lower part of chron 4n.2n. This means that the duration of only part of this cycle must have been at least 185 ky. The base of cycle six is just above the lowest datum indicating chron 4n.2n polarity and continues to the top of DS1A, a sequence boundary with little stratigraphic evidence for missing record. Using the entire duration of chron 4n.2n yields a maximum duration of 422 ky for cycle 6. These data suggest that through time, rates of relative sea-level change may have been decreasing with increasing duration of sea-level cycles (Fig. 6). Alternatively, rates of sea-level change may have remained rapid with duration of sea-level cycles remaining constant (Fig. 6). In this scenario, the upper fining-upward cycles were deposited during times when sea-level cycles left little obvious sedimentary record because of the overall high sea-level position and increased area or number of drowned substrates (Fig. 7; see Discussion section for more explanation).

The lack of pinning points in DS2 precludes calculation of rates of rises and falls of relative sea level. Although pinning points indicate a relative sea-level fall of at least 100 m associated with MB2 and its subaerial exposure, it is not known how much time it took for this fall to occur. However, the entire time for MB2 accumulation plus the length of time for exposure and downlap on MB2 gives a minimum rate of 22.7 cm/ky for the 100 m fall.

For DS3, sea level had to rise enough to flood the MB2 subaerial exposure surface and eventually deposit reef-crest facies 130 m upslope (Figs. 3, 6). Initial DS3 deposits are part of chron 3Ar. The rate of sea-level rise for these strata can be bracketed in several ways using the total relative rise of 150 m, from the basal unconformity to the top of the aggraded reef-crest facies of chron 3Ar. Integrating the 150 m rise over the total time of chron 3Ar and the 406 ky of the unconformity results in a rate of 19 cm/ky; using only the time for chron 3Ar results in a rate of sea-level rise of 40.8 cm/ky (Fig. 6).

In chron 3An.2n, DS3 strata largely are progradational with a possible downstepping component. Reef-crest facies, just after the start of the chron, drop in elevation about 30 m to reef-core facies at the end of the chron. Pomar's (1991) model suggests a depth of 5 to 30 m for the reef-core facies. These data indicate that relative sea level during 3An.2n was either stable or fell by a rate of up to 8.4 cm/ky (Fig. 6).

During chron 3An.1r, reefs prograded and downstepped. The amount of sea-level fall can be estimated by using Pomar's (1991) model to estimate a depth of 5–30 m for reefal carbonates and an elevation fall of approximately 30 m from the top of the reef near the start of the chron to the top of reef-crest facies near the end of the chron. These data suggest a relative fall in sea level of 5–55 m to produce a rate of fall of 3.8–41.0 cm/ky (Fig. 6).

Deposits of chron 3An.1n also downstep and prograde. The earliest reefs were deposited in water depths of 5–30 m (model of Pomar 1991); later reef deposits, 19 m lower in elevation, have facies indicating deposition in 5–10 m of water (model of Pomar 1991). Thus, the overall relative fall in sea level was between 14 and 44 m, which yields rates of fall of between 5.8 and 18 cm/ky (Fig. 6).

For each of the four cycles of the TCC, pinning points indicate relative sea-level rises and falls of at least 25–30 m (Franseen et al. 1993; Goldstein and Franseen 1995). Using a conservative estimate for TCC duration of 400–100 ky, for reasons discussed earlier, and assuming symmetrical cycles with linear sea-level change, minimum rates of relative sea-level change lie between 25 and 120 cm/ky (Fig. 6). These conservative rates fall within the range measured for Holocene glacio-eustatic rates (Kendall and Schlager 1981).

DISCUSSION

Comparison of Local Relative Sea Level to Eustatic Curves

Quantitative relative sea-level curves for our study area have been produced in previous studies using the pinning-point method (Franseen et al. 1993; Goldstein and Franseen 1993; Goldstein and Franseen 1995). The paleomagnetic data, combined with the radiometric age data from the volcanic unit in DS1A and the likely age of TCC strata, allow for quantitative time calibration of the relative sea-level curves (Fig. 6). This calibration reveals that the carbonate complex spans approximately 3.3 my, and that the five depositional sequences developed from third-order (1–10 my) and fourth-order (0.1–1.0 my) scale relative sea-level changes with higher-frequency events superimposed.

Time calibration of the pinning-point relative sea-level curve allows for comparison with global eustatic records. Figure 6 shows two versions of the Haq et al. (1988) global eustatic curve; one is the curve as originally presented and the other is the same curve recalibrated to the new GPTS of Cande and Kent (1995). Using the original eustatic curve, comparison to our relative sea-level curve shows a poor match, but this is to be expected because they are calibrated to different time scales. The new chron ages of Cande and Kent (1995) suggest a shift downward of approximately 700 ky to recalibrate the curve. Other studies have used new magnetostratigraphy, strontium isotope, biostratigraphy, and oxygen isotope data to revise ages for some sequences on the Haq et al. (1988) curve (e.g., for the Oligocene to middle Miocene, Miller et al. 1996). With the new calibration, our sequences correlate with TB3.2, TB3.3, and TB3.4. The comparison of curves suggests a global influence, at least on third-order local sea-level history, including the third-order drop associated with the downstepping reefs in DS3, which are the basin-margin representation of events leading up to the Messinian salinity crisis.

DS1B through MB2, and DS3 appear to be third-order sequences. DS1A may be part of the same third-order sequence as DS1B (the relative sea-level fall at the end of DS1A could be a higher-frequency event) or DS1A may be the topmost part of a separate third-order sequence. DS2 is a fourth-order sequence. The fining-upward cycles in the lowest chron of DS1B result from at least fifth-order (0.01– 0.1 my) but likely higher-frequency cycles of sea-level change. Cycles within DS3 may result from fourth-order or higher-frequency sea-level changes. The TCC appears to result from a fourth-order sea-level cycle and its internal cycles are at least fifth order but are likely higher-frequency cycles.

Finally, rates of rises and falls calculated for the parts of our curves that correlate to third-order scale rises and falls are generally higher than those normally associated with third-order rises and falls (1–10 cm/ky; Kendall and Schlager 1981), as are the magnitudes of our rises and falls compared with the Haq et al.(1988) curve. Our curve also shows higher-frequency events ($>$ third order) whereas the Haq et al. (1988) curve smooths out the high-frequency events by incorporating only the highest positions of higher-order fluctuations to produce the lower overall amplitudes and rates for third-order-scale fluctuations. Further, sequence boundaries between the two curves differ. The differences described above should be expected because our curve is a relative sea-level curve in contrast to a eustatic curve, such as that of Haq et al. (1988).

It is useful to compare the pinning-point curve to higher-frequency records of eustatic sea-level change, one of which would be the record of glacial ice volume reflected in the stable isotopes of marine carbonate. For this time interval, detailed isotope records exist from 7.7 Ma to the beginning of the Pliocene (Miller et al 1991; Kastens 1992; Hodell et al 1994; Shackleton et al 1995; Shackleton and Hall, in press). The best detailed isotopic data exist for the interval from 6.9 Ma to 5.8 Ma, where there is

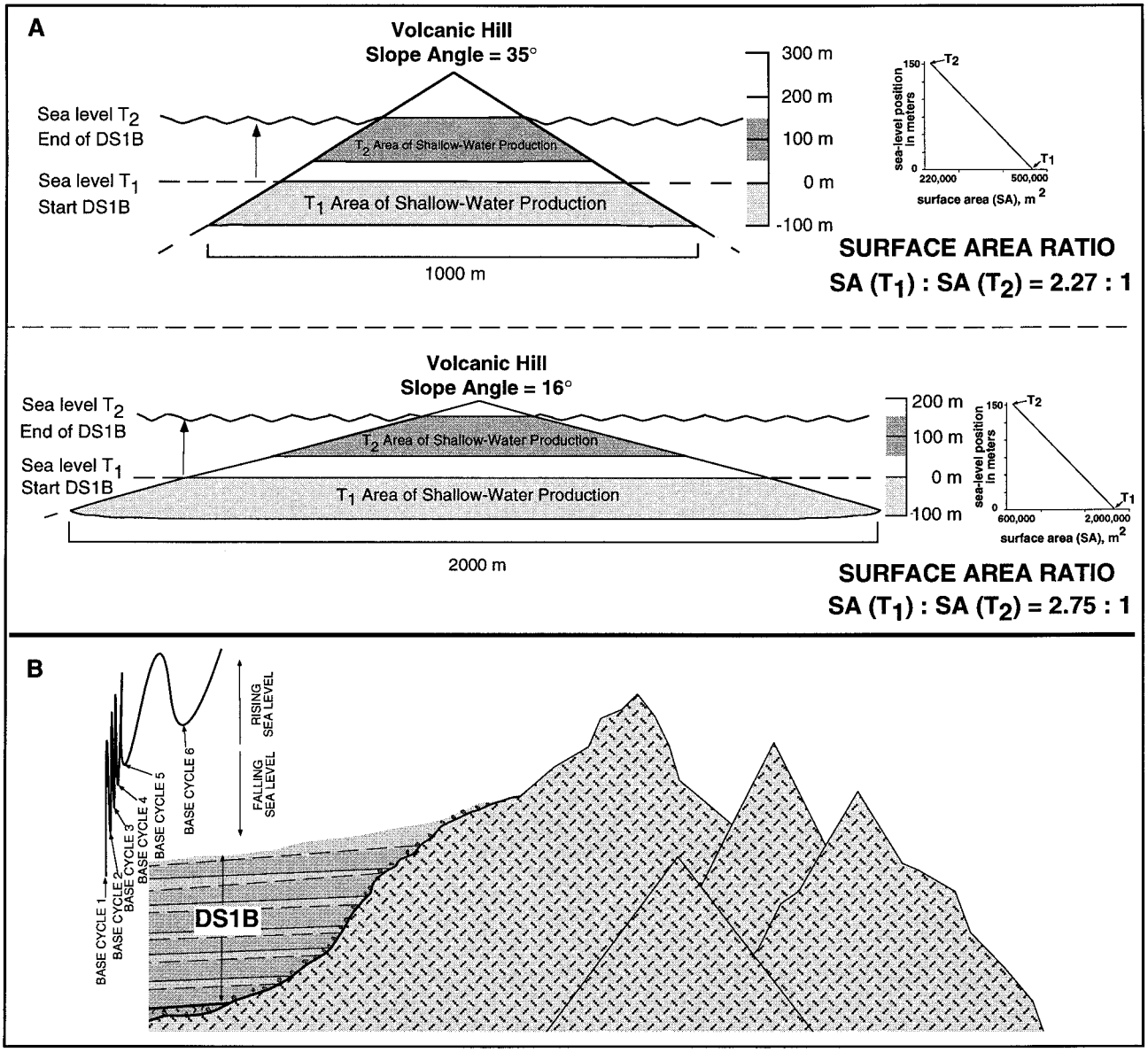

FIG. 7.—**A)** Model showing decreasing area for shallow-water carbonate production (assumed to be < 100 m water depth in this scenario) on conical volcanic substrate during the 150 m relative sea-level rise of DS1B; the shallow-water carbonate sediment was bypassed to gently sloping toes of slopes (< 15°) to form bypass ramps (not shown). Two examples are provided to show a range of representative morphologies and elevations of volcanic highs in the study area. The upper example illustrates a 250-m-high volcanic hill with slope angle of 35°, and the lower example illustrates a 186-m-high volcanic hill with slope angle of 16°. Note that the plots in both examples show the linear decrease in substrate surface area for shallow-water production with rising sea level. From the start of DS1B (T1) to the end of DS1B (T2), the surface area for shallow-water production decreased by a factor of 2.27 for the upper example and by a factor of 2.75 for the lower example. We interpret the decrease in surface area available for shallow-water production during the DS1B sea-level rise to have contributed to the decreasing accumulation rate from the base to the top of DS1B. **B)** Model showing the increased area of drowned substrate during the overall DS1B sea-level rise. We interpret this increased area of drowned substrate from the beginning to end of DS1B to have contributed to the upward-decreasing accumulation rate of DS1B.

strong evidence for spectral variation interpreted to result from global ice volume varying near the 41 ky obliquity and 100 ky eccentricity cycles (Hodell et al. 1994; Shackleton and Hall, in press). This time interval coincides with deposition of DS3 reef cycles, at least some of the sea-level variation of which could be interpreted as responding to glacio-eustasy.

For the interval from 5.8 Ma to about 5.3 Ma (TCC time), the isotopic record is much less readily interpretable (Shackleton et al. 1995; Shackleton and Hall, in press). To the best of our knowledge, for strata older than 7.7 Ma (which include DS1A and DS1B), highly detailed isotope records have not yet been published. However, the isotopic variability (Miller et al. 1991), evidence for ice growth from 10 to 8 Ma (Miller et al 1987), and an equivocal glacial event at 8.5 Ma (Wright and Miller 1992) suggest that glacio-eustasy remains a probable driver for some sea-level changes in DS1A and DS1B.

Quantification of Controls on Platform Development

DS1A and DS1B Ramp Strata

Accumulation Rates.—The overall rates at which the cool-water ramp sediments of DS1B accumulated generally decrease from an initial rate of > 15.6 cm/ky to about 2 cm/ky. These slow rates are consistent with other accumulation rates measured for modern cool-water shelf carbonates (Enos

1991; Boreen and James 1993). Similar rates also have been reported for Tertiary cool-water carbonates from other areas. James and Von der Borch (1991) reported vertical accretion at a rate of 1.3 cm/ky since the middle Oligocene on the Eucla platform, southern Australia. Boreen and James (1995) reported rates of $<$ 5 cm/ky for Oligo-Miocene cool-water carbonates exposed along the Victoria coast of southeastern Australia. Rates up to 24 cm/ky since the middle Miocene for shelf carbonates off of New Zealand were reported in Carter (1988).

Although it would be tempting to interpret the consistent decrease in accumulation rates in DS1B as a response due solely to deepening water during the documented relative rise in sea level of at least 150 m, the decreasing rates do not correlate perfectly with increasing thicknesses of deeper-water (foraminiferal wackestone) lithologies (Figs. 4, 5; Franseen et al. 1997). Alternatively, the decline in accumulation rates may be due to the effects of decreasing area of shallow-water sediment production through time. If the volcanic basement substrate is modeled as a series of conical hills, then the substrate area in shallow water would have progressively decreased during the DS1B relative rise in sea level. Because much of the sediment of DS1B had been produced on upslope substrates and subsequently bypassed downslope to sites of permanent accumulation, a decrease in area for carbonate production during the rise would have resulted in a slower accumulation rate.

We have modeled the effect of decreasing area of shallow-water carbonate production (assumed to be $<$ 100 m water depth in this scenario) on conical substrates (volcanic hills) during the 150 m relative sea-level rise during DS1B deposition (Fig. 7A). Two substrates were modeled to simulate the range of morphologies, elevations, and slope angles of the volcanic basement highs observed in the field. One example illustrates a volcanic hill 250 m high with a slope angle of 35° (Fig. 7A). In this example the surface area for shallow-water carbonate production decreases by a factor of 2.27 during the 150 m relative rise in sea level. The other example illustrates a volcanic hill 186 m high with a slope angle of 16° (Fig. 7A). For this example, the surface area for shallow-water carbonate production decreases by a factor of 2.75 during the 150 m relative rise in sea level. If the area of shallow-water substrate can be regarded as a proxy for sediment production, then it appears that on a bypass ramp like DS1B, accumulation rates can be controlled by relative sea-level changes that directly affect the area for shallow-water carbonate production. However, this cannot be the only cause for the decrease in accumulation rate observed in DS1B because the actual decrease in accumulation rate from the base to the top of DS1B is by a factor of eight, in contrast to the factor of two or three predicted by the model.

A complementary role may be played by the ''drowning'' of shallow-water substrates as well as unknown complex factors of sediment dispersal involved in bypass. During the 150 m relative rise in sea level of DS1B, it is likely that many of the shallow-water substrate areas were progressively drowned (Figs. 7B). These areas no longer were able to supply significant sediment to bypass downslope, and thus, the overall accumulation rate downslope would have decreased.

Rates of Sea-Level Fluctuations.—For DS1A and DS1B, the long-term rates of relative sea-level rise (DS1A through DS1B is 17.6 cm/ky; DS1B minimum rate is 21.4 cm/ky; Fig. 6) are greater than the accumulation rates. Normally, this discrepancy should have resulted in drowning of the DS1B ramp, as has been shown for similar types of Miocene ramp strata (e.g., Simone and Carannante 1988; Carannante and Simone 1996) and which is typical for carbonate ramps during rapid base-level rises (Burchette and Wright 1992). However, the bypass origin and high-frequency sea-level signals suggest that it would have been difficult to drown these ramps completely. First, they are bypass ramps, built from sediment that was bypassed downslope, as well as sediment that accumulated in place. Given the high volcanic substrates adjacent to the ramp, even during the highest sea level documented for DS1B, some substrates existed in the zone of shallow-water carbonate production to produce sediment to be bypassed down to the area of ramp formation (Fig. 7B). Second, there were high-frequency, high-amplitude sea-level changes superimposed on the long-term relative rise in sea level. In the fining-upward cycles produced by these sea-level changes, the hemipelagic limestones argue for temporary drowning of the ramp, but the red-algae-rich packstones and grainstones argue for reinitiation of the ramp at low points of the high-frequency sea-level cycles.

Two alternative models can be formulated for the sea-level history in DS1B. The fining-upward cycles in the lowest chron within DS1B average less than 54 ky/cycle, but cycles in the later chrons yield an apparent time per cycle of at least 185 ky to no more than 422 ky. The lowest four of the six cycles are generally the thickest and were deposited in the shortest period of time. One explanation is that the duration of high-frequency sea-level cycles slowed during DS1B deposition (Fig. 6). Another explanation is that high-frequency sea-level cycles were of $\leq$ 54 ky duration throughout the deposition of DS1B (Fig. 6), and with sea level so high during the later part of DS1B, the platform remained drowned for most of the high-frequency sea-level cycles. The only sea-level cycles that would have deposited sedimentary cycles would have been those in which sea level reached a position low enough to initiate deposition of red algal facies.

The fining-upward cycles in DS1B have been interpreted to result from deepening upward (Franseen et al 1996). Similar facies have been observed in association with incipient drowning in transgressive systems tracts (Burchette and Wright 1992). The average cycle duration for DS1B may have been $\leq$ 54 ky with rates of relative sea-level change between 111 cm/ky and 260 cm/ky (Fig. 6). The gradational upward transition from shallower-water RAPG to deeper-water (mostly pelagic) FGWP facies indicates deepening and drowning of the ramp. The sharp contact between the FGWP facies and overlying RAPG facies of the subsequent cycle could indicate an abrupt event of shallowing. A scenario of rapid relative falls in sea level followed by slower relative rises in sea level could explain these cycle characteristics for all six DS1B cycles (Fig. 8A).

An alternative, and geologically more feasible, explanation is that the six fining-upward cycles may have resulted from high-frequency symmetrical sea-level cycles which produced sedimentary cycles that were asymmetric because of a lag-time component (a finite period of time before carbonate production reaches its full potential; Schlager 1981). In this scenario (Fig. 8B), at the highest sea-level position of a high-frequency cycle, the carbonate ramp surface and upslope volcanic substrate areas are in deep water and only pelagic deposits are accumulating. As sea level falls at a high rate of at least 111 cm/ky, and likely much higher, upslope volcanic substrate areas begin to enter the shallower-water window of RAPG productivity, but sedimentation is not initiated because of lag time. With time, sea level falls far enough to expose the ramp surface to the window of RAPG productivity but production still has not started because of lag time. Eventually RAPG production starts, near the lowest point of the high-frequency sea-level cycle (Fig. 8B), and it does so rapidly (cf. Enos 1991) and at a high volume because sediment can be produced from the entire relatively broad area of the carbonate ramp surface as well as adjacent upslope volcanic substrate source areas. This produces a sharp contact between FGWP and overlying RAPG sediment. During the subsequent relative rise in sea level, lag time is unimportant because areas of RAPG sediment productivity are merely shut off consecutively as productive sediment substrates are progressively drowned. The result is the upward gradation from RAPG to FGWP facies (Fig. 8B).

DS2 Strata

Accumulation Rates.—Our correlation to the GPTS produces minimum accumulation rates of 3.5 to $>$ 11.2 cm/ky for DS2 and MB2. These deposits represent the transition from cool-water ramp facies of DS1B to warm-water reef facies of DS3. However, the accumulation rates are not simply intermediate between the two as one might predict. This suggests

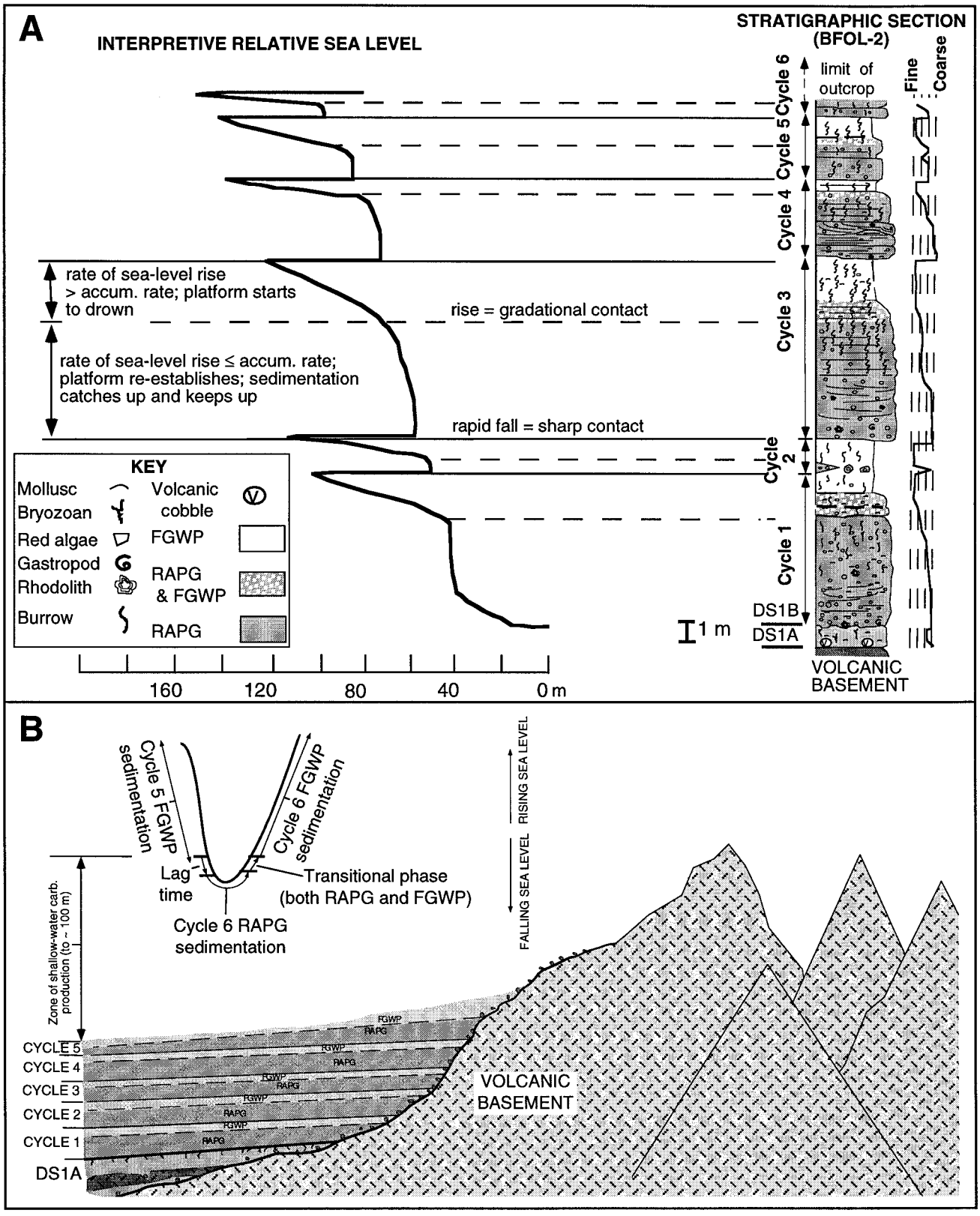

FIG. 8.—**A)** Model of rapid relative falls in sea level followed by slower relative rises in sea level creating the six DS1B cycles. **B)** Alternative, and geologically more feasible, explanation for the six fining-upward cycles resulting from high-frequency symmetrical relative sea-level cycles that incorporate a lag-time component into sediment accumulation (see text for explanation). Cross section illustrates start of Cycle 6. Sea-level curve illustrates change in sedimentation on the ramp as sea level falls from a high point of Cycle 5 through the low point and rise of Cycle 6.

that controls other than simple climate change must be important in controlling accumulation rate.

Rates of Sea-Level Fluctuations.—Rates of sea-level change cannot easily be calculated for DS2 because of the lack of pinning points. However, it has already been shown that MB1, at the base of DS2, is a megabreccia associated with a relative fall in sea level. The stratigraphic and magnetic data show little evidence for nondeposition or large-scale erosion suggesting that the relative change in sea level associated with MB1 may have been rapid and of short duration. Similarly for the MB2 megabreccia at the top of DS2, stratigraphic and magnetic data show little evidence for nondeposition or large-scale erosion at the base of MB2 suggesting rapid deposition of reef material downslope during a relative fall in sea level. The subaerial-exposure surface capping MB2 deposits in distal slope positions indicates that sea level continued to drop after MB2 deposition, which provides supporting evidence of megabreccia transport during early stages of falling sea level.

DS3 Reef Complex Strata

Accumulation Rates.—As shown earlier, the presence of three full chrons (3An.2n, 3An.1r, 3An.1n) and most of another (3Ar) in DS3 strata (Fig. 3) allows us to examine proxies for vertical accumulation rate and progradation patterns for the reef complex in some detail.

Our calculated vertical accumulation rates for DS3 (ranging from 10.3 cm/ky to 21.8 cm/ky) are similar to rates reported for other tropical Miocene carbonates. Equivalent-age strata of the Natuna Platform, South China Sea, have accumulation rates that range from 8.5 cm/ky to 19.7 cm/ky (Sarg 1988; Rudolph and Lehmann 1989). Upper Eocene to lower Miocene strata of Enewetak have rates of 17.0 cm/ky and 7.6 cm/ky, respectively (Saller 1984). Middle Miocene to Holocene strata of the northern Great Barrier Reef have vertical accumulation rates of 6.7 cm/ky to 10.0 cm/ky (Davies 1988). It is important to realize that although these rates are similar, they may not be directly comparable, because of variation in the location of the measurements on the shelf or slope, and in some studies, vertical measurements through dipping slope strata.

Comparing the influence of relative sea-level change to accumulation rates is useful. The strata falling within the first chron of DS3 have the highest accumulation rate. During this chron, there is evidence for a significant rise in sea level over an area of low paleoslope. This low-gradient substrate had been created by deposition of earlier sequences. Thus, when sea level initially rose, a broad shallow-water area was available for carbonate production. In addition, the climate had warmed towards tropical conditions (Franseen and Goldstein 1996; Franseen et al. 1997), thereby creating a system conducive to high carbonate productivity. As sea level continued to rise, additional accommodation allowed continued productivity over this broad area. Eventually, the accommodation was filled and reef facies began prograding. The combination of a relative rise in sea level to create accommodation and a broad area of productivity likely resulted in the highest rates of accumulation. The strata in all of the subsequent chrons in DS3 exhibit evidence of a relative fall in sea level that resulted in progradation and downstepping of reef complexes. It is not surprising that the strata in these later chrons had lower accumulation rates because accommodation was being eliminated and, as sea level fell across steep forereef slope topography, the area for shallow-water carbonate production decreased.

Progradation Rates.—Strata within the first chron of DS3 were deposited during a relative sea-level rise of at least 130 m (Figs. 3, 6; Franseen et al. 1993; Goldstein and Franseen 1995). Those strata initially aggraded and then prograded with steep (25–35°) downlapping clinoforms (Franseen 1989; Franseen and Goldstein 1996). The low progradation rate (0.39 km/my) is not surprising given the significant aggradational component. Aggradation of the reefal strata suggests that productivity was sufficient for sedimentation to keep up with relative rise in sea level. Later progradation suggests that sediment accumulation was more rapid than the rate of sea-level rise.

Later DS3 reef strata correspond to chrons 3An.2n, 3An.1r, and 3An.1n and have progradational and downstepping geometries, which indicate stable and falling relative sea level (Figs. 3, 6). Progradation rates are 1.02 km/my, 1.45 km/my, and 1.21 km/my, respectively. Stable to falling relative sea level limited aggradation, which resulted in increased lateral progradation compared to the first chron in DS3. Significant progradation was possible only because the earlier sequences had filled in much of the deeper-water areas, allowing clinoforms to prograde into a relatively shallow-water basin (typically 40–60 m and no deeper than 80 m). If reefs had grown on a steeper margin, within a deeper basin, progradation rate would have been lower because of the greater volume of sediment necessary to form a complete clinoform. If the margin was too steep, no progradation would have occurred until the depositional slope was in equilibrium.

The overall progradation rate calculated for the DS3 reefal platform is 0.90 km/my (ranging from 0.39 km/my to 1.45 km/my) and can be compared to other platforms in different settings. The leeward margin of the northwest Bahamas platform has prograded at a rate of 2.7 km/my since middle Miocene time (James and Von der Borch 1991). Even with the deep basin into which these strata have prograded, these rapid rates must be a function of dispersal of the high volume of sediment produced by the enormous area of bank top of the Bahamas (Eberli and Ginsburg 1989). In our area, progradation was slow despite the shallow basin over which progradation occurred. This is best explained by the comparatively tiny area of shallow-water production and the discontinuous nature of reef growth in this setting or reefs fringing volcanic highs during progressively falling sea level.

The progradation in our study area can also be compared to other upper Miocene carbonate platforms in the western Mediterranean. The Mallorca platform shows two contrasting styles of progradation for reef-complex strata (Pomar and Ward 1995; Pomar et al. 1996). Although correlations between our reef-complex strata and those of Mallorca are not precise, it appears that the two reef complexes are generally age equivalent (Franseen and Mankiewicz 1991; Pomar 1991). On Mallorca, a barrier-reef complex prograded as much as 20 km to the southwest over a broad shallow carbonate platform, with later phases only 25–50 m deep (Pomar and Ward 1995; Pomar et al. 1996). Because the depth of the basin there was similar to that in our study area, overall sediment production around southwest Mallorca must have been higher because of the wide sediment production area in extensive lagoons (Pomar and Ward 1995; Pomar et al. 1996) and fewer breaks in reef production. However, along the margin of the Palma basin of Mallorca, the surface onto which the reefal platform prograded was relatively deep (about 200 m) and lagoons were less extensive, so progradation there was less than 2 km (Pomar and Ward 1995; Pomar et al. 1996). The Cabo de Gata reef progradation is similar in scale to the Palma basin margin. Both areas lack extensive regions of backreef sediment production, but the Palma basin platform was forced to prograde into deeper water. This suggests that overall productivity was higher for the Palma basin margin than in Cabo de Gata. Comparatively high productivity at Mallorca may have been controlled by its more open marine setting, which was more isolated from the effects of nutrients and clastics that appeared to repeatedly interrupt carbonate production in the archipelago setting of the Cabo de Gata area.

The Melilla platform in northern Morocco provides another example for comparison. It displays an upper Miocene reef complex (Cunningham 1995) that correlates to the later stages of our reef complex (Farr et al., unpublished data). This reefal platform prograded across a substrate, possibly with relatively steep erosional topography (see Figure 5 of Cunningham 1995). Despite this erosional topography, the reefal clinoforms prograded over a relatively shallow-water substrate (5–60 m; Cunningham 1995) similar to that in our study area. The progradation rate at Melilla was 1.9 km/my (Cunningham 1995), intermediate between the Cabo de

Gata average progradation rate at 0.90 km/my and that of the Bahamian platform at 2.7 km/my (James and Von der Borch 1991). Even though the Melilla platform prograded over a shallow-water substrate, its comparatively slow progradation rate must in part be due to its lack of extensive bank-top carbonate production. The higher progradation rate of Melilla reefs compared to those in Cabo de Gata may be because the setting of the Melilla reefs precluded the interruption of carbonate production from clastic influx and runoff that was so common in the Cabo de Gata area.

Rates of Sea-Level Fluctuations.—DS3 clinoforms downlap from less than one to just several meters above MB2 or its correlative surface (sequence boundary). The best data available (basal DS3 unconformity to the end of chron 3Ar) suggests that the rate of relative sea-level rise above this sequence boundary must have been much greater than 19 cm/ky (Fig. 6). Downlap onto this surface suggests that the rate of sea-level rise was too rapid to produce a transgressive systems tract.

Earliest DS3 deposits of chron 3Ar were initially aggradational and became progradational (highstand systems tract) during an overall relative sea-level rise roughly estimated to be 13.6 cm/ky (Fig. 6). This value provides an estimate that may be applicable for aggradational and progradational deposits of highstand systems tracts in general.

Younger DS3 deposits are progradational and downstepping and represent a transition from a highstand to a forced regressive systems tract. During the initial chron (3An.2n) in these younger DS3 deposits, relative sea level was stable or fell by a rate up to 8.4 cm/ky, during the next chron (3An.1r) relative sea level fell at rates of 3.8 to 41.0 cm/ky, and during the last complete chron of DS3 (3An.1n) the rate of relative fall was between 5.8 and 18.0 cm/ky (Fig. 6). These data illustrate that rates of fall of approximately 10 cm/ky or less were conducive to generation of forced regressive systems tracts in these reefal systems.

Terminal Carbonate Complex (TCC)

Accumulation Rates.—A duration of between 400 ky and 100 ky for TCC deposition (for reasons discussed earlier) yields overall accumulation rates of 7.5 to 30.0 cm/ky. Because that estimate includes time for cycle-bounding surfaces of subaerial exposure, accumulation rates within each cycle were likely much more rapid. Overall rapid rates for accumulation (cf. Enos 1991) are consistent with the shallow-water conditions for TCC cycles and rapid rates of sea-level change, consistent with the rapid addition of accommodation.

Rates of Sea-Level Change.—The duration of 400 to 100 ky for TCC deposition yields an average calculated cycle duration between 100 and 25 ky for the four preserved cycles. Whereas it would be tempting to invoke Milankovitch forcing as the control for these cycle durations, our data do not allow us to make this assertion because we do not know if all cycles are of the same duration. In addition, other sedimentary cycles may exist downslope (beneath present-day Mediterranean sea level) and be equivalent to the upslope cycle boundaries (deposition downslope during upslope subaerial exposure).

Pinning points indicate that relative sea-level rises and falls of 25–30 m occurred during deposition of each cycle (Franseen et al. 1993). Using the 100 to 400 ky estimate for TCC duration and assuming symmetrical cycles with linear sea-level change, the data indicate rates of relative sea-level rises and falls between 25 and 120 cm/ky (Fig. 6). These conservative rates fall within the range measured for Holocene glacio-eustatic rates (Kendall and Schlager 1981). Our ability to correlate TCC strata in our area with TCC strata in other areas of the western Mediterranean using paleomagnetic data (e.g., Sorbas basin and the Melilla area in northeastern Morocco; Farr et al., unpublished data) suggests at least regional controls on TCC deposition. The paleomagnetic data show that the four TCC cycle boundaries correlate to a similar number of subaerial exposure surfaces at Niue in the South Pacific (Lu et al. 1996). Further, widespread distribution of similar numbers of ''TCC-style'' cycles of approximately the same age (e.g., Roca 1986; Cunningham 1995; Calvet et al. 1996; Esteban 1996; Esteban et al. 1996; Lu et al. 1996), suggests a possible global control on sea-level change responsible for TCC cycles. The rates and amplitudes of the sea-level change argue for a glacio-eustatic origin.

Implications For Sequence Stratigraphy

The paleomagnetic data presented in this paper allow us to go beyond our previous sequence-stratigraphic work in the Cabo de Gata area and to analyze the effects of rates of relative sea-level change in conjunction with paleoslope and climate. The combination of these data provides an opportunity to evaluate, quantitatively, the conditions under which classical sequence stratigraphy and systems-tract models may or may not be applicable.

Overall, our study indicates that when shallow-water conditions intersect areas of high substrate slope ($> 15°$ in our area), independently of climate, location and internal architecture of carbonate platforms are controlled by the location of gently sloping substrates and processes of bypass. Whereas the location and architecture are not directly linked to sea-level position, sea-level history and rates influence facies patterns.

For example, the DS1B temperate-water ramp represents an entire fourth-order depositional sequence that was deposited during a minimum long-term rate of relative rise in sea level between 17.6 and 21.4 cm/ky. It would be tempting to interpret DS1B as a transgressive systems tract, but DS1B is an entire depositional sequence, the onlap of which is clearly not ''coastal onlap''. This onlap does not reflect a direct base-level control; when sea level intersects steep slopes ($> 15°$ in our area), bypass processes dominate, resulting in accumulation and onlap of sediment at toes of slopes (Figs. 7, 8, 9). Additionally, sedimentologic evidence from the fining-upward cycles of DS1B suggests that they were caused by higher-frequency relative changes in sea level of 30–70 m or more. At least for the lower part of the DS1B depositional sequence, the cycles were generated from relative changes in sea level of at least 111 cm/ky to even > 260 cm/ky. Our data suggest that such higher-frequency, rapid sea-level fluctuations result in bypass ramps formed at toes of slopes and composed of fining-(deepening-) upward cycles that preserve no recognizable systems-tract characteristics.

The chlorozoan facies in the two megabreccias (MB1 and MB2) show that the potential existed to build rigid frameworks in DS2. However, steep-sloped substrates ($> 15°$) and rapid (> 22.7 cm/ky) relative sea-level falls resulted in complete erosion of DS2 reefs from upslope positions and their downslope redeposition as megabreccias on gently sloping substrates. These stratiform deposits are in stark contrast to the downstepping clinoform-geometry reefs in DS3 deposited during a later relative fall in sea level, suggesting that steep slopes and rapid sea-level falls may not be conducive to development of forced regressive systems tracts with downstepping clinoform geometries. The data from our study also suggest that only a short duration of lowstand may be necessary to form these megabreccias and that they may be deposited rapidly during early stages of falling sea level. Because reef megabreccias can also form from other processes, including highstand shedding, bypass during relative sea-level fall is best confirmed by identifying reef material that overlies deeper water facies *and* is capped by a surface of subaerial exposure (MB2) or contains clasts with evidence of exposure prior to downslope transport (MB1).

In contrast to characteristics of DS1B and DS2, DS3 deposits illustrate that if carbonate sediments are generated when shallow-water conditions exist over substrates of low slope ($< 15°$ in our area), then geometries of deposits may fit at least partially with systems-tract, sequence-stratigraphy models in which depositional sequence geometries, stacking patterns, and facies are largely controlled by the relative position of sea level. However, our data indicate that rates of relative sea-level change are important for determining if systems tracts develop under these conditions, and if so, of what type.

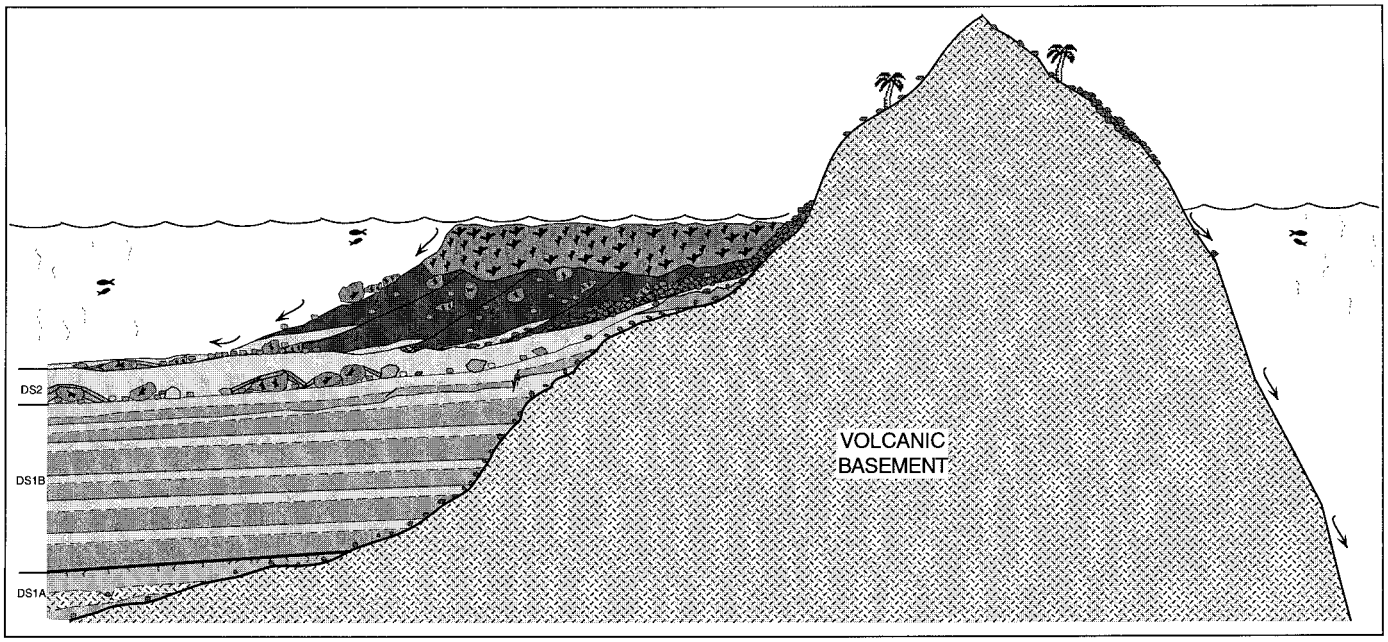

FIG. 9.—Schematic cross section illustrating the nature of DS3 deposits and their relation to substrate paleoslope and earlier deposits. No scale or specific period of reef development is implied. The figure illustrates that where substrate slopes were steep, no deposits accumulated. Preservation of in-place DS3 reef strata was dependent on earlier bypass deposits of DS1A, DS1B, and DS2, which accumulated in deeper water at toes of slopes. These deposits created gentle slopes for development and preservation of DS3 reefs. Steep-sloped areas lacking DS1A, DS1B, and DS2 deposits did not permanently preserve DS3 deposits.

DS3 contains reefal platform deposits that developed when sea-level position was just above areas of gentle paleoslope. These conditions create a broad area of productivity over a substrate slope gentle enough that materials are not easily bypassed across it, creating the best possibility for permanent preservation of in-place reef with constructional topography (Fig. 9). These reefs are characterized by aggradational to progradational geometries directly responding to sea-level position. Although DS3 represents an entire third-order depositional sequence (Fig. 6), no transgressive systems tract is recognizable. Our data suggest that the rate of relative rise of sea level ($\gg$ 19 cm/ky) initiating DS3 might have been too rapid to form a transgressive systems tract. Furthermore, latest DS3 strata form a forced regressive systems tract (Hunt and Tucker 1992) characterized by downstepping reefs that were deposited during the relative fall in sea level at the end of DS3. In addition to favorable paleoslope conditions, our data indicate that slow rates of sea-level fall ($<$ 10 cm/ky) are important for generation of forced regressive systems tracts with downstepping reef clinoform geometries. Faster rates of sea-level fall may be more likely to result in reef megabreccias similar to MB1 and MB2.

Each TCC cycle essentially drapes 25–30 m of topography and does not form geometries typical of classical systems tracts. Each of the TCC cycles can be considered a high-frequency ($\geq$ fifth-order) depositional sequence (each bounded by evidence for relative sea-level fall). If the exposures in our area are extensive enough to be representative for these high-order sequences, it appears that sea-level changes of 25–120 cm/ky were too rapid to generate typical systems tracts. Perhaps, such rapid changes were more conducive to formation of cycles that drape minor topography where relatively flat topography and shallow water coincided.

CONCLUSIONS

(1) Combined sequence stratigraphy, quantitative relative sea-level history, and magnetostratigraphy provide high-resolution quantitative constraints for upper Miocene temperate- to warm-water carbonate depositional sequences developed in a setting of variable substrate paleoslope. These result in one of the highest-resolution chronostratigraphies to date for shallow-water Miocene carbonate sequences and allow us to identify the global and glacio-eustatic influences on development of depositional sequences at third-order to $>$ fifth-order scales.

(2) Substrate paleoslope and rates of sea-level fluctuations are dominant and combine with sea-level position to control sequence location and architecture. Climate is a relatively minor control in comparison.

(3) Where shallow-water conditions intersect areas of high substrate slope ($>$ 15° in our area), location and architecture of carbonate sequences are controlled by location of gently sloping substrates and processes of bypass. Sea-level control is subordinate under these conditions, and typical systems-tract, sequence-stratigraphy models are not likely to apply. Carbonate sediments generated in shallow-water conditions on substrates of low slope ($<$ 15° in our area) are likely to be affected largely by relative sea-level history. Therefore, depositional sequence geometries, stacking patterns, and facies of carbonates deposited under these conditions may fit well with systems-tract, sequence-stratigraphy models. Only under these conditions, of shallow water over a flat substrate, can shallow-water carbonate cycles, typical of many carbonate platforms, develop.

(4) Rates of sea-level fluctuations are an important influence on depositional sequence architecture. Even where gently sloping substrates are in shallow water, rapid rates of sea-level change (19 to 260 cm/ky) may preclude formation of systems tracts at third-order to fifth-order and higher scales. Rates of sea-level fluctuations also influence patterns of sediment accumulation and progradation. Slow rates of relative sea-level fall ($<$ 10 cm/ky in our study) across favorable paleoslope are likely necessary for development of forced regressive systems tracts with downstepping reef clinoform geometries. In areas of steep substrate paleoslope, rates of sea-level fluctuations are likely to be subordinate to bypass processes, but may influence internal facies patterns and, in conjunction with complex dispersal patterns, the resultant accumulation rates. Rates of relative sea-level fall ($>$ 21.7 cm/ky in our study) across steep paleoslope facilitate processes of bypass, independently of climate and the ability to build rigid frameworks.

(5) Methods used in this paper result in the development of quantitative models that integrate different data, including accumulation, progradation,

and sea-level rates. These models provide predictive capabilities for sequence-stratigraphic studies of cool- and warm-water carbonates developed in settings characterized by variable substrate paleoslopes, such as steeply erosional or constructional platform margins, archipelagos, island arcs, or other oceanic island settings. Because such topography is likely on most types of carbonate platforms, our results may have specific applications to studies of carbonate ramps and platforms throughout much of the geologic record.

ACKNOWLEDGMENTS

This research was supported by a National Science Foundation research grant (EAR-9527004) and a Dupont/Conoco Educational Aid Grant. The results presented here are part of an ongoing research program that has benefited from discussions over the years with A. Arribas, Jr., S. Dorobek, M. Esteban, N.P. James, W.J. Meyers, E.J. Oswald, L. Pomar, J.-M Rouchy, J.F. Sarg, W. Schlager, A. Simo, and W.B. Ward and, especially, L.C. Pray. J.-M. Rouchy provided valuable comments on an earlier version of this manuscript. JSR reviewers W.A. Morgan, S. Phillips, and W.B. Ward are thanked for detailed reviews that helped us clarify our ideas. We thank J.B. Southard for his suggestions and careful editing of the manuscript.

REFERENCES

Addicott, W.D., Snavely, P.D., Jr., Bukry, D., and Poore, R.Z., 1978, Neogene stratigraphy and paleontology of southern Almeria Province, Spain: An overview: U.S. Geological Survey, Bulletin 1454, 49 p.

Aissaoui, D.M., McNeil, D.F., and Hurley, N.F., eds., 1993, Applications of Paleomagnetism to Sedimentary Geology: SEPM, Special Publication 49, 216 p.

Aissaoui, D.M., McNeil, D.F., and Kirschvink, J.L., 1990, Magnetostratigraphic dating of shallow water carbonates from Mururoa atoll, French Polynesia: implications for global eustasy: Earth and Planetary Science Letters, v. 97, p. 102–112.

Boreen, T.D., and James, N.P., 1993, Holocene sediment dynamics on a cool-water carbonate shelf: Otway, Southeastern Australia: Journal of Sedimentary Petrology, v. 63, p. 574–588.

Boreen, T.D., and James, N.P., 1995, Stratigraphic sedimentology of Tertiary cool-water limestones, SE Australia: Journal of Sedimentary Research, v. B65, p. 142–159.

Burchette, T.P., and Wright, V.P., 1992, Carbonate ramp depositional systems: Sedimentary Geology, v. 79, p. 3–57.

Calvet, F., Zamarreño, I., and Vallés, D., 1996, Late Miocene reefs of the Alicante—Elche basin, southeast Spain, *in* Franseen, E.K., Esteban, M., Ward, W.C., and Rouchy, J.-M., eds., Models for Carbonate Stratigraphy from Miocene Reef Complexes of the Mediterranean Regions: SEPM, Concepts in Sedimentology and Paleontology Series no. 5, p. 177–190.

Cande, S.C., and Kent, D.V., 1995, Revised calibration of the geomagnetic polarity time scale for the Late Cretaceous and Cenozoic: Journal of Geophysical Research, v. 100, p. 6093–6096.

Carannante, G., and Simone, L., 1996, Rhodolith facies in the central–southern Apennine Mountains, Italy, *in* Franseen, E.K., Esteban, M., Ward, W.C., and Rouchy, J.-M., eds., Models for Carbonate Stratigraphy from Miocene Reef Complexes of the Mediterranean Regions: SEPM, Concepts in Sedimentology and Paleontology Series no. 5, p. 261–276.

Carter, R.M., 1988, Post-breakup of the Kaikoura Synthem (Cretaceous–Cenozoic), continental margin, southeastern New Zealand: New Zealand Journal of Geology and Geophysics, v. 31, p. 405–429.

Channell, J.E.T., Torii, M., and Hawthorne, T., 1990, Magnetostratigraphy of sediments recovered at sites 650, 651, 652, and 654 (Leg 107, Tyrrhenian Sea), *in* Kastens, K.A., and Mascle, J., eds., Ocean Drilling Program, Proceedings, Scientific Results, v. 107, p. 335–346.

Clauzon, G., Suc, J.-P., Gautier, F., Berger, A., and Loutre, M.-F., 1996, Alternate interpretation of the Messinian salinity crisis: Controversy resolved?: Geology, v. 24, p. 363–366.

Cunningham, K.J., 1995, An upper Miocene sedimentary succession, Melilla basin, northeastern Morocco [unpublished Ph.D. thesis]: University of Kansas, 371 p.

Cunningham, K.J., Farr, M.R., and Rakic–El Bied, K., 1994, Magnetostratigraphic dating of an upper Miocene shallow-marine and continental sedimentary succession in northeastern Morocco and correlation to regional and global events: Earth and Planetary Science Letters, v. 127, p. 77–93.

Davies, P.J., 1988, Evolution of the Great Barrier Reef—reductionist dream or expansionist vision: Sixth International Coral Reef Symposium, Townsville, Australia, Proceedings, vol. 1, p. 9–17.

Eberli, G.P., and Ginsburg, R.N., 1989, Cenozoic progradation of northwestern Great Bahama Bank, A record of lateral platform growth and sea-level fluctuations, *in* Crevello, P.D., Wilson, J.L., Sarg, J.F., and Read, J.F., eds., Controls on Carbonate Platform and Basin Development: SEPM, Special Publication 44, p. 339–351.

Enos, P., 1991, Sedimentary parameters for computer modeling, *in* Franseen, E.K., Watney, W.L., Kendall, C.G.St.C, and Ross, W.C., eds., 1991, Sedimentary Modeling: Computer Simulations and Methods for Improved Parameter Definition: Kansas Geological Survey, Bulletin 233, p. 63–100.

Esteban, M., 1996, An overview of Miocene reefs from the Mediterranean area: General trends and facies models, *in* Franseen, E.K., Esteban, M., Ward, W.C., and Rouchy, J.-M., eds., Models for Carbonate Stratigraphy from Miocene Reef Complexes of the Mediterranean Regions: SEPM, Concepts in Sedimentology and Paleontology Series no. 5, p. 3–54.

Esteban, M., 1979, Significance of upper Miocene coral reefs of the western Mediterranean: Palaeogeography, Palaeoclimatology, Palaeoecology, v. 29, p. 169–188.

Esteban, M., Braga, J.C., Martin, J.M., and Santisteban, C., 1996, Western Mediterranean reef complexes, *in* Franseen, E.K., Esteban, M., Ward, W.C., and Rouchy, J.-M., eds., Models for Carbonate Stratigraphy from Miocene Reef Complexes of the Mediterranean Regions: SEPM, Concepts in Sedimentology and Paleontology Series no. 5, p. 55–72.

Franseen, E.K., 1989, Depositional sequences and correlation of middle to upper Miocene carbonate complexes, Las Negras area, southeastern Spain [unpublished Ph.D. thesis]: University of Wisconsin–Madison, 374 p.

Franseen, E.K., and Goldstein, R.H., 1992, Sequence stratigraphy of Miocene strata, Las Negras area, southeastern Spain: Implications for quantification of relative change in sea level, *in* Franseen, E.K., Goldstein, R.H., Braga, J.C., Martin, J.M., eds., A Guidebook for the Las Negras and Sorbas areas, SEPM/IAS research conference on carbonate stratigraphic sequences: Sequence boundaries and associated facies, La Seu, Spain, August 30–September 3, p. 1–77.

Franseen, E.K., and Goldstein, R.H., 1996, Paleoslope, sea level and climate controls on upper Miocene platform evolution, Las Negras area, southeastern Spain, *in* Franseen, E.K., Esteban, M., Ward, W.C., and Rouchy, J.-M., eds., Models for Carbonate Stratigraphy from Miocene Reef Complexes of the Mediterranean Regions: SEPM, Concepts in Sedimentology and Paleontology Series no. 5, p. 159–176.

Franseen, E.K., and Mankiewicz, C., 1991, Depositional sequences and correlation of middle(?) to late Miocene carbonate complexes, Las Negras and Nijar areas, southeastern Spain: Sedimentology, v. 38, p. 871–898.

Franseen, E.K., and Mankiewicz, C., 1993, Depositional sequences and correlation of middle (?) to late Miocene carbonate complexes, Las Negras and Nijar areas, southeastern Spain: Reply: Sedimentology, v. 40, p. 353–356.

Franseen, E.K., Goldstein, R.H., and Farr, M.R., 1997, Substrate-slope and climate controls on carbonate ramps: Revelations from upper Miocene outcrops, SE Spain, *in* James, N.P., and Clarke, J., eds., Cool-Water Carbonates: SEPM, Special Publication 56, p. 271–290.

Franseen, E.K., Goldstein, R.H., and Whitesell, T.E., 1993, Sequence stratigraphy of Miocene carbonate complexes, Las Negras area, Southeastern Spain: Implications for quantification of changes in relative sea level, *in* Loucks, R.G., and Sarg, J.F., eds., Carbonate Sequence Stratigraphy: Recent Developments and Applications: American Association of Petroleum Geologists, Memoir 57, p. 409–434.

Gautier, F., Clauzon, G., Suc, J-P., Cravatte, J., and Violanti, D., 1994, Age et durée de la crise de salinité messinienne: Académie des Sciences [Paris], Comptes Rendus, v. 318, p. 1103–1109.

Gianniny, G.L., and Simo, J.A., 1996, Implications of unfilled accommodation space for sequence stratigraphy on mixed carbonate–siliciclastic platforms: an example from the lowest Desmoinesian (Middle Pennsylvanian), southwest Paradox basin, Utah, *in* Longman, M.W., and Sonnenfeld, M.D., eds., Paleozoic Systems of the Rocky Mountain Region: SEPM, Rocky Mountain Section, p. 213–234.

Goldhammer, R.K., Harris, M.T., Dunn, P.A., and Hardie, L.A., 1993, Sequence stratigraphy and systems tract development of the Latemar platform, Middle Triassic of the Dolomites (Northern Italy): Outcrop calibration keyed by cycle stacking patterns, *in* Loucks, R.G., and Sarg, J.F., eds., Carbonate Sequence Stratigraphy: Recent Developments and Applications: American Association of Petroleum Geologists, Memoir 57, p. 353–388.

Goldstein, R.H., and Franseen, E.K., 1993, Pinning points: A method that provides quantitative constraints on relative sea-level history (abstract): American Association of Petroleum Geologists, Abstracts with Programs, p. 109.

Goldstein, R.H., and Franseen, E.K., 1995, Pinning points: A method that provides quantitative constraints on relative sea-level history: Sedimentary Geology, v. 95, p. 1–10.

Grammer, G.M., Eberli, G.P., van Buchem, F.S.P., Stevenson, G.M., and Homewood, P., 1996, Application of high-resolution sequence stratigraphy to evaluate lateral variability in outcrop and subsurface—Desert Creek and Ismay intervals, Paradox Basin, *in* Longman, M.W., and Sonnenfeld, M.D., eds., Paleozoic Systems of the Rocky Mountain Region: SEPM, Rocky Mountain Section, p. 235–266.

Handford, C.R., and Loucks, R.G., 1993, Carbonate depositional sequences and systems tracts responses of carbonate platforms to relative sea-level changes, *in* Loucks, R.G., and Sarg, J.F., eds., Carbonate Sequence Stratigraphy: Recent Developments and Applications: American Association of Petroleum Geologists, Memoir 57, p. 3–42.

Haq, B.U., Hardenbol, J., and Vail, P.R., 1988, Mesozoic and Cenozoic chronostratigraphy and cycles of sea-level change, *in* Wilgus, C.K., Hastings, B.S., Kendall, C.G.St.C., Posamentier, H.W., Ross, C.A., and Van Wagoner, J.C., eds., Sea Level Changes—An Integrated Approach: SEPM, Special Publication 42, p. 72–108.

Hilgen, F.J., and Langereis, C.G., 1993, A critical evaluation of the Miocene/Pliocene boundary as defined in the Mediterranean: Earth and Planetary Science Letters, v. 118, p. 167–179.

Hodell, D.A., Benson, R.H., Kent, D.V., Boersma, A., and Rakic–El Bied, K., 1994, Magnetostratigraphic, biostratigraphic, and stable isotope stratigraphy of an upper Miocene drill core from the Salé Briqueterie (northwestern Morocco): A high-resolution chronology for the Messinian stage: Paleoceanography, v. 9, p. 835–855.

Hunt, D., and Tucker, M.E., 1992, Stranded parasequences and the forced regressive wedge systems tract: deposition during base-level fall: Sedimentary Geology, v. 81, p. 1–9.

James, N.P., and Clarke, J.A.D., eds., 1997, Cool-Water Carbonates: SEPM, Special Publication 56, 440 p.

James, N.P., and Von der Borch, C.C., 1991, Carbonate shelf edge off southern Australia: A prograding open-platform margin: Geology, v. 19, p. 1005–1008.

Kastens, K.A., 1992, Did glacio-eustatic sea level drop trigger the Messinian salinity crisis?

New evidence from ocean drilling program site 654 in the Tyrrhenian sea: Paleoceanography, v. 7, p. 333–356.

KENDALL, C.G.ST.C., AND SCHLAGER, W., 1981, Carbonates and relative changes in sea level: Marine Geology, v. 44, p. 181–212.

KIRSCHVINK, J.L., 1980, The least-squares line and plane and the analysis of palaeomagnetic data: Geophysical Journal of the Royal Astronomical Society, v. 62, p. 699–718.

LOWRIE, W., AND HELLER, F., 1982, Magnetic properties of marine limestones: Reviews of Geophysics and Space Physics, v. 20, p. 171–192.

LU, G., AHARON, P., WHEELER, C.W., AND MCCABE, C., 1996, Magnetostratigraphy of the uplifted former atoll of Niue, South Pacific: implications for accretion history and carbonate diagenesis: Sedimentary Geology, v. 105, p. 259–274.

MCNEILL, D.F., GINSBURG, R.N., CHANG, S.-B.R., AND KIRSCHVINK, J.L., 1988, Magnetostratigraphic dating of shallow-water carbonates from San Salvador, Bahamas: Geology, v. 16, p. 8–12.

MILLER, K.G., FAIRBANKS, R.G., AND MOUNTAIN, G.S., 1987, Tertiary oxygen isotope synthesis, sea level history, and continental margin erosion: Paleoceanography, v. 2, p. 1–19.

MILLER, K.G., MOUNTAIN, G.S., THE LEG 150 SHIPBOARD PARTY, AND MEMBERS OF THE NEW JERSEY COASTAL PLAIN DRILLING PROJECT, 1996, Drilling and dating New Jersey Oligocene–Miocene sequences: Ice volume, global sea level, and Exxon records: Science, v. 271, p. 1092–1095.

MILLER, K.G., WRIGHT, J.D., AND FAIRBANKS, R.G., 1991, Unlocking the ice house: Oligocene–Miocene oxygen isotopes, eustasy, and margin erosion: Journal of Geophysical Research, v. 96, p. 6829–6848.

MONTENAT, C., OTT D'ESTEVOU, P., AND MASSE, P., 1987, Tectonic–sedimentary characters of the Betic Neogene basins evolving in a crustal transcurrent shear zone (SE Spain): Centre Recherche Exploration–Production, Elf-Aquitaine, Bulletin, v. 11, p. 1–22.

POMAR, L., 1991, Reef geometries, erosion surfaces and high-frequency sea-level changes, upper Miocene reef complex, Mallorca, Spain: Sedimentology, v. 38, p. 243–269.

POMAR, L., AND WARD, W.C., 1995, Sea-level changes, carbonate production and platform architecture: The Llucmajor Platform, Mallorca, Spain, *in* Haq, B.U., ed., Sequence Stratigraphy and Depositional Responses to Eustatic, Tectonic and Climatic Forcing: Dordrecht, The Netherlands, Kluwer Academic Publishers, p. 87–112.

POMAR, L., WARD, W.C., AND GREEN, D.G., 1996, Upper Miocene reef complex of the Llucmajor Area, Mallorca, Spain, *in* Franseen, E.K., Esteban, M., Ward, W.C., and Rouchy, J.-M., eds., Models for Carbonate Stratigraphy from Miocene Reef Complexes of the Mediterranean Regions: SEPM, Concepts in Sedimentology and Paleontology Series no. 5, p. 191–226.

QUINN, T.M., AND MATTHEWS, R.K., 1990, Post-Miocene diagenetic and eustatic history of Enewetak Atoll: Model and data comparison: Geology, v. 18, p. 942–945.

REID, S.K., AND DOROBEK, S.L., 1993, Sequence stratigraphy and evolution of progradational, foreland carbonate ramp, Lower Mississippian Mission Canyon Formation and stratigraphic equivalents, Montana and Idaho, *in* Loucks, R.G., and Sarg, J.F., eds., Carbonate Sequence Stratigraphy: Recent Developments and Applications: American Association of Petroleum Geologists, Memoir 57, p. 327–352.

ROCA, D.V., 1986, Carbonate facies and depositional cycles in the upper Miocene of Santa Pola (Alicante, S.E. Spain): Revista d'Investigacions Geologiques, v. 42/43, p. 45–66.

ROUCHY, J.-M., 1982, La genèse des évaporites messiniennes de Méditerranée: Muséum National d'Histoire Naturelle, Mémoires, v. 50, 267 p.

ROUCHY, J.-M., AND SAINT MARTIN, J.-P., 1992, Late Miocene events in the Mediterranean as recorded by carbonate–evaporite relations: Geology, v. 20, p. 629–632.

RUDOLPH, K.W., AND LEHMANN, P.J., 1989, Platform evolution and sequence stratigraphy of the Natuna platform, south China Sea, *in* Crevello, P.D., Wilson, J.L., Sarg, J.F., and Read, J.F., eds., Controls on Carbonate Platforms and Basin Development: SEPM, Special Publication 44, p. 353–364.

SALLER, A.H., 1984, Diagenesis of Cenozoic limestones on Enewetak Atoll [unpublished Ph.D. thesis]: Louisiana State University, Baton Rouge, Louisiana, 363 p.

SARG, J.F., 1988, Carbonate sequence stratigraphy, *in* Wilgus, C.K., Hastings, B.S., Kendall, C.G.St.C., Posamentier, H.W., Ross, C.A., and Van Wagoner, J.C., eds., Sea-Level Changes—An Integrated Approach: SEPM, Special Publication 42, p. 154–181.

SCHLAGER, W., 1981, The paradox of drowned reefs and carbonate platforms: Geological Society of America, Bulletin, v. 92, p. 197–211.

SERRANO, F., 1992, Biostratigraphic control of Neogene volcanism in Sierra de Gata (southeast Spain): Geologie en Mijnbouw, v. 71, p. 3–14.

SHACKLETON, N.J., AND HALL, M.A., in press, The late Miocene stable isotope record, site 926: Ocean Drilling Program, Proceedings, Scientific Results.

SHACKLETON, N.J., HALL, M.A., AND PATE, D., 1995, Pliocene stable isotope stratigraphy of site 846: Ocean Drilling Program, Proceedings, Scientific Results, v. 138, p. 337–355.

SIMONE, L., AND CARANNANTE, G., 1988, The fate of foramol (''temperate-type'') carbonate platforms: Sedimentary Geology, v. 60, p. 347–354.

SONNENFELD, M.D., AND CROSS, T.A., 1993, Volumetric partitioning and facies differentiation within the Permian Upper San Andres Formation of Last Chance Canyon, Guadalupe Mountains, New Mexico, *in* Loucks, R.G., and Sarg, J.F., eds., Carbonate Sequence Stratigraphy: Recent Developments and Applications: American Association of Petroleum Geologists, Memoir 57, p. 435–474.

WRIGHT, J.D., AND MILLER, K.G., 1992, Miocene stable isotope stratigraphy, site 747, Kerguelen Plateau: Ocean Drilling Program, Proceedings, Scientific Results, v. 120, p. 855–866.

Received 9 December 1996; accepted 5 November 1997.